Predicted Reaction Rates of $H_xN_yO_z$ Intermediates in the Oxidation of Hydroxylamine by Aqueous Nitric Acid

Robert W. Ashcraft,[†] Sumathy Raman,[‡] and William H. Green*,[†]

Department of Chemical Engineering, Massachusetts Institute of Technology, Cambridge, Massachusetts 02139, and Department of Chemistry, Oakwood College, Huntsville, Alabama 35896

This work reports computed rate coefficients of 90 reactions important in the autocatalytic oxidation of hydroxylamine in aqueous nitric acid. Rate coefficients were calculated using four approaches: Smoluchowski (Stokes–Einstein) diffusion, a solution-phase incarnation of transition state theory based on quantum chemistry calculations, simple Marcus theory for electron-transfer reactions, and a variational TST approach for dissociative isomerization reactions that occur in the solvent cage. Available experimental data were used to test the accuracy of the computations. There were significant discrepancies between the computed and experimental values for some key parameters, indicating a need for improvements in computational methodology. Nonetheless, the 90-reaction mechanism showed the ability to reproduce many of the trends seen in experimental studies of this very complicated kinetic system. This work highlights reactions that may govern the system evolution and branching behavior critical to the stability of the system. We hope that this analysis will guide experimental investigations to reduce the uncertainties in the critical rate coefficients and thermochemistry, allowing an unambiguous determination of the dominant reaction pathways in the system. Advances in efficient and accurate solvation models that effectively separate entropic and enthalpic contributions will most directly benefit solution-phase modeling efforts. Methods for more accurately estimating activity coefficients, including at infinite dilution in multicomponent mixtures, are needed for modeling high ionic strength aqueous systems. A detailed derivation of the solution-phase equilibrium and transition state theory rate expressions in solution is included in the Supporting Information.

Introduction

The construction of complex chemical-physical models in the absence of experimental data is a continuing goal of the scientific and engineering community. If accurate enough, these predictive models could be used to design new systems, avoiding much of the expensive Edisonian experimentation that slows innovation. Even when the predictive models are not accurate enough for design, they can still be useful for identification of key reaction paths and to help guide experimental studies. In many cases, it is the inability to predict thermochemical data and rate coefficients accurately that has limited the success of such attempts. Ideally, one would like to build an entire mechanism based solely on ab initio calculations that is capable of making reliable predictions. In the gas phase, this is becoming possible for some systems if one makes use of all available tools, including those that use microcanonical rate constants over many energy levels to accurately predict rate coefficients as a function of temperature and pressure. There is a large community devoted to developing these methods, and much has been published demonstrating their accuracy and applicability. In recent years, a number of highly complex and very successful chemical kinetic models have been constructed for gas-phase C/H/N/O systems.[1,2] For example, predictive kinetic models based on quantum chemical calculations identified the true pathway by which $CH + N_2$ leads to NO_x formation,[3,4] the pathway to NO_x

formation through NNH in low-*T* flames,[5,6] and the autocatalytic pathway in methane pyrolysis.[7] However, predicting condensed-phase chemical kinetics has proven much more difficult due to the lack of accurate, computationally efficient quantum solvation models.

The current methods suitable for "quickly" predicting the behavior of multicomponent reacting systems are generally limited to continuum solvation methods that ignore specific solute/solvent interactions and treat the solvent as a continuum dielectric. These continuum models are parametrized to some degree, whether in the atomic radii, nonelectrostatic interactions, or other empirical corrections. It is also possible to perform various molecular dynamics (MD) or hybrid quantum mechanics/molecular mechanics (QM/MM) simulations that specifically treat solute/solvent interactions in an attempt to gain better accuracy. However, these methods are inherently slow due to the computation power required to perform the calculations rigorously, and it would be difficult at present to use these methods to generate the volume of data necessary to build a complex, solution-phase reaction mechanism with hundreds of reactions. Another possible approach to solution-phase predictions is to combine the relatively ideal nature of the existing continuum models with activity coefficients estimated in another manner. The recently developed COSMO-RS theory of Klamt has been shown to accurately predict the activity coefficients and phase equilibrium behavior of a variety of simple systems.[8–10] This method is also parametrized and is based on ab initio calculations for a molecule, combined with the statistical mechanics of interacting surfaces, which allows for the estimation of chemical potentials and activity coefficients. However,

* Corresponding author. E-mail: whgreen@mit.edu. Phone: +1.617.253.4580. Fax: +1 0.617.324.0066.
† Massachusetts Institute of Technology.
‡ Oakwood College. Present address: Exxon-Mobil Research and Engineering Co., Route 22 East, Annandale, NJ.

TABLE 1: Previously Proposed Autocatalytic and Scavenging Reaction Mechanisms

$$2(H^+ + NO_3^- + HONO \overset{fast}{\rightleftharpoons} N_2O_4 + H_2O)$$
$$NH_2OH + N_2O_4 \overset{slow}{\rightarrow} HNO + N_2O_3 + H_2O$$
$$HNO + N_2O_4 \rightarrow HONO + N_2O_3$$
$$2(N_2O_3 + H_2O \overset{fast}{\rightleftharpoons} 2HONO)$$
$$\overline{NH_2OH + 2HONO_2 \rightarrow 3HONO + H_2O}$$

$$H^+ + HONO \rightleftharpoons NO^+ + H_2O$$
$$NO^+ + NH_3OH^+ \rightleftharpoons NH_3ONO^+ + H^+$$
$$NH_3ONO^+ \rightarrow ONNH_2OH^+$$
$$ONNH_2OH^+ \rightarrow HONNOH + H^+$$
$$HONNOH \rightarrow N_2O + H_2O$$
$$\overline{NH_3OH^+ + HONO \rightarrow N_2O + 2H_2O}$$

the applicability of COSMO-RS to highly ionic systems and transition state structures is as yet unproven.

Here, the rate coefficients for a variety of reactions of $H_xN_yO_z$ molecules, radicals, and ions in aqueous solution are estimated using continuum solvation models and density functional theory. The computed thermochemistry for most of these species was presented earlier.[11] An attempt is also made to reproduce the experimental data available for the nitric acid, nitrous acid, and hydroxylamine ($HONO_2/HONO/NH_2OH$) aqueous system using a detailed chemical model based on these computed rate and thermochemical parameters. We also examine the accuracy of the methodologies used in estimating model parameters and comment on the importance of each contribution to creating a successful kinetic model.

The reactions following the addition of hydroxylamine to nitric acid are thought to have led to several explosions during nuclear material reprocessing. A number of experimental studies have been conducted on this system, the most notable of which are those by Pembridge and Stedman[12] and Bourke and Stedman.[13] They proposed concise autocatalytic[12] and scavenging[13] mechanisms that can explain the observed behavior in the limited temperature and composition ranges studied, as seen in Table 1.

The proposed autocatalytic reaction mechanism, which describes the pathway for the production of up to three excess moles of nitrous acid per autocatalytic cycle, can be seen to be a nonelementary reaction mechanism and is highly speculative. The mechanism is said to be consistent with the experimental data, which was taken at 298 K and with the absorbance of HONO at 372 nm being the main observable. In the practical application of this process, the temperatures will typically be in the 300−330 K range, with particular interest in the behavior near the explosive instability at the upper end of the temperature range. With such a simple model and the limited amount and range of the data, one cannot confidently extrapolate this model far from the experimental range.

The scavenging of HONO was examined by Bourke and Stedman, and a nearly elementary reaction mechanism was proposed.[14] They showed that with reasonable assumptions about the rapid equilibria of two reactions, the model and experimental data can be consistent. They were not able to extract kinetic data for most of the reactions; however, they did postulate that at 298 K the rate coefficient for the reaction of NO^+ and NH_3OH^+ was 6×10^6 M^{-1} s^{-1} at low acidities. This estimate was based on the simplistic proposed model, along with other assumptions about what reactions were in equilibrium and which was rate-limiting.

These previous works provide a basis for building an elementary reaction mechanism that will detail each step in the process and ideally will allow more reliable predictions outside the range of the experimental data. However, to create an elementary reaction mechanism, thermochemical and kinetic data are needed, which creates a problem given the lack of solution-phase data. Limited data are available for acid−base equilibria and solution-phase equilibria of several of the NO_x species, with rate coefficient data available for select reactions,

usually at a single temperature. Ab initio calculations are required to fill the many gaps in the data. As such, we rely heavily on quantum chemical estimates of thermochemical and rate coefficients in this work.

Computation Methodology

Thermochemistry Estimation. The thermochemical parameters were estimated using the Gaussian03 suite of programs, along with additional corrections to account for important contributions missing from the Gaussian03 output. A very brief summary of the methodology is given here; a more in-depth explanation can be found elsewhere, where many of the important details and numerical values are given.[11] The solution-phase thermochemical data were estimated using a combination of high-level gas-phase thermochemistry calculations and continuum solvation model (IEFPCM) estimates of the solvation free energy. Aqueous solvation free energies were obtained using the IEFPCM/B3LYP/6−311G(2d,d,p) level of theory with the UAHF radii set. Full geometry optimizations and frequency calculations were completed for all molecules. The solution-phase enthalpy of formation was calculated by taking the gas-phase value and adding the solvation enthalpy, as in eq 1. The solvation enthalpy was derived from the ab initio solvation free energy and the estimated solvation entropy.[11]

$$\Delta H_f^{soln,298K} = \Delta H_{f,CBSQB3}^{gas,0K} + \int_{0K}^{298K} C_{p,gas-like}\, dT + \Delta H_{solv}^{298K} \tag{1}$$

$$S_{solution}^{298K} = S_{gas}^{298K} + \Delta S_{solv,cav}^{298K} + \Delta S_{solv,emp}^{298K} \tag{2}$$

The entropy of each species in solution was estimated as a combination of the gas-phase entropy, the solvation entropy due to cavitation ($\Delta S_{solv,cav}^{298K}$), and an empirical solvation entropy term ($\Delta S_{solv,emp}^{298K}$) based on solute bonding. Typical values of the cavitation and empirical solvation entropies range from −10 to −25 cal/(mol K) and −2 to +5 cal/(mol K), respectively. The Gibbs free energy for each species in solution was calculated from the enthalpy and entropy in solution. When any system is modeled, the stable species thermochemistry is generally of the utmost importance because it is used to determine equilibrium concentrations and reverse rate coefficients. Specifically, the accuracy of the solvation free energy and understanding its partitioning between entropic and enthalpic contributions are critical to a successful model.

Rate Coefficient Estimation. Rate coefficients in the forward (exothermic) direction were estimated in one of four ways. The majority were estimated either as diffusion-limited for barrierless reactions or using transition state theory (TST) for reactions with significant barriers. Several electron-transfer reactions were also included in the mechanism and were treated using Marcus theory. A handful of other reactions were classified as reactions in a solvent cage and were estimated in a manner that will be described in more detail below. Reverse rate coefficients were calculated using the equilibrium constant to ensure thermodynamic consistency throughout the mechanism. The expression

Oxidation of Hydroxylamine by Aqueous Nitric Acid

J. Phys. Chem. A, Vol. 112, No. 33, 2008 **7579**

for the equilibrium constant is given in eq 3, where ΔG^o_{Rxn} is the standard state free energy change of reaction, C^o_i is the standard state concentration of species i, $C^o_{T,i}$ is the total solution concentration at the standard state for species i, $C^\#_T$ is the total solution concentration at the actual state of the mixture, and $\gamma_i^{+\rightarrow\#}$ and $\gamma_i^{+\rightarrow o}$ are the activity coefficients to correct from the reference state to the actual and standard states, respectively. A detailed description of the assumptions made in deriving eq 3 are outlined in a writeup of common equilibrium expressions in solution thermodynamics that is included in the Supporting Information. Equation 4 is the expression used to calculate the reverse rate coefficient. The equations used to estimate the forward rate coefficients are discussed in the following sections.

$$K_C = \exp\left(\frac{-\Delta G^o_{\text{Rxn}}}{RT}\right)\left(\frac{\prod\limits_{\text{products}} C^o_i \frac{C^\#_T}{C^o_{T,i}}}{\prod\limits_{\text{reactants}} C^o_i \frac{C^\#_T}{C^o_{T,i}}}\right) \cdot \left(\frac{\prod\limits_{\text{reactants}} \frac{\gamma_i^{+\rightarrow\#}}{\gamma_i^{+\rightarrow o}}}{\prod\limits_{\text{products}} \frac{\gamma_i^{+\rightarrow\#}}{\gamma_i^{+\rightarrow o}}}\right) \quad (3)$$

$$k_r = \frac{k_f}{K_C} \quad (4)$$

Accurate estimation of reaction barriers is always important to building a successful model. It is likely that with improved solvation models, barrier estimates will also become more accurate. However, another important aspect in solution-phase systems is understanding reaction types unique to condensed phases and devising new methodologies to estimate rate coefficients. One such example is the effect of solvent cage on reactions, as is discussed below.

Diffusion Limited Reactions. Approximately half of the proposed reactions are radical−radical recombination, cation−anion recombination, or simple proton transfers and were assumed to be diffusion-limited. This assumption is supported by data found in the Notre Dame Radiation Laboratory's aqueous kinetics database, which generally shows rate coefficients between 10^9 and 10^{10} L mol^{-1} s^{-1} for radical recombination reactions. The diffusivity-dependent encounter rate of two species and Stokes−Einstein diffusion within the solvent were used to estimate these rate coefficients.[15] The viscosity of the $HONO_2$−H_2O system was required and varies significantly with both the temperature and concentration of nitric acid. These effects were taken into account through a multivariate expression; see the Supporting Information for more information. Proton-transfer and radical recombination reactions were assumed to be diffusion limited, neglecting any small barriers that may be present. The true nature of the aqueous proton is unclear, and it was assumed that H_3O^+ is a good representation. From an energetic standpoint this is reasonable, but the diffusivity of H_3O^+ and H^+ in water will be significantly different due to the ability of the proton to "hop" through the solvent.[16] To capture this discrepancy, when the diffusion-limited rate coefficients are computed, the effective radius of the hydronium ion was changed from the calculated value of 1.88 Å to 0.25 Å to match the experimental proton diffusivity of $\sim 1 \times 10^{-8}$ m^2 s^{-1} at 298 K.[17]

Transition State Theory. Transition states (TS) in solution were optimized in Gaussian03 using the same basis set and method as in the solution-phase thermochemical calculations. A simple Wigner tunneling correction was included in the rate coefficient estimates. Many of the radical reactions and neutral species reactions in solution are functionally identical to their gas-phase counterparts; however, several reactions required explicit solvent molecules to be used in the transition

structure to allow for proton transfer to the solvent. In general, water-assisted H-transfer reactions proceed with a significantly lower barrier than their unassisted counterparts, due to less "strain" in the TS complex when the water molecule(s) are present. In all cases where an explicit water molecule was used in the transition state, it was also included in one of the reactant structures to minimize basis set superposition error.

The solution-phase transition state theory rate coefficient expression for a bimolecular reaction is given by eq 5 or 6, which are identical (see Supporting Information for derivations). In these equations, κ includes the tunneling effects, C^o_i is the standard state concentration, Q^o_i and V^o_i are the partition function and molar volume evaluated under standard state conditions, $\gamma_i^{+\rightarrow o}$ and $\gamma_i^{+\rightarrow\#}$ represent the activity coefficients needed to convert from the reference behavior to the standard state or actual behavior, $\Delta G^o_{\text{TS,soln}}$ is the standard state free energy of activation in solution, $\Delta E^{0K}_{\text{TS,gas}}$ is the gas-phase reaction barrier with zero point energies included, and $\Delta\Delta G^*_{\text{solv,TS}}$ is the change in constant-concentration solvation free energy of the transition state relative to the reactants. It was assumed that the total concentration terms in eq 3 cancel because they vary by less than 15% over the entire range studied here. The total solution-phase concentration for aqueous $HONO_2$ mole fractions of 0.1 and 0.2 are 51.6 and 47.5 M.[18]

$$k_{\text{TST}} = \kappa \frac{k_B T}{h} \exp\left(\frac{-\Delta G^o_{\text{TS,soln}}}{RT}\right)\left(\frac{C^o_{\text{TS}}}{C^o_A C^o_B}\right)\left(\frac{\gamma^{+\rightarrow o}_{\text{TS}}}{\gamma^{+\rightarrow\#}_{\text{TS}}} \frac{\gamma^{+\rightarrow\#}_A}{\gamma^{+\rightarrow o}_A} \frac{\gamma^{+\rightarrow\#}_B}{\gamma^{+\rightarrow o}_B}\right)$$

(5)

$$k_{\text{TST}} = \overbrace{\kappa \frac{k_B T}{h}\left(\frac{\frac{Q^o_{TS}}{V^o_{TS}}}{\frac{Q^o_A}{V^o_A}\frac{Q^o_B}{V^o_B}}\right)\exp\left(\frac{-\Delta E^{0K}_{TS,\text{gas}}}{RT}\right)}^{k_{TST}(gas)\ using\ C^o_{i,\,gas}} \cdot$$

$$\overbrace{\exp\left(\frac{-\Delta\Delta G^*_{solv,TS}}{RT}\right)\left(\frac{\gamma^{+\rightarrow o}_{TS}}{\gamma^{+\rightarrow o}_A \gamma^{+\rightarrow o}_B}\right)\left(\frac{\gamma^{+\rightarrow\#}_A \gamma^{+\rightarrow\#}_B}{\gamma^{+\rightarrow\#}_{TS}}\right)}^{at\ C^o_{i,\,soln}} \quad (6)$$

The $\Delta\Delta G^*_{\text{solv,TS}}$ term is defined as $\Delta G^*_{\text{solv,TS}} - (\Delta G^*_{\text{solv,A}} + \Delta G^*_{\text{solv,B}})$, where $\Delta G^*_{\text{solv,i}}$ is defined as the free energy change for moving a mole of gas into solution when the concentration is equal to $C^*_{\text{i,soln}}$ in both phases. Each $\Delta G^*_{\text{solv,i}}$ term implicitly includes the nonideal contributions present in the both phases at the standard state concentration; here the gas phase was assumed to behave ideally. For more details on these equations, please see the Supporting Information.

Ideally, the activity coefficients of all species and transition states should be estimated to provide the most accurate rate data, but they are difficult to determine accurately in complex solutions. The COSMO-RS theory proposed by Klamt[8–10,19–21] potentially allows one to estimate the activity coefficient of any species or TS for which an electronic structure calculation can be performed. It utilizes the statistical thermodynamics of interacting surfaces to calculate the chemical potential of interaction of the solute and solvent mixture, and the activity coefficients are derived from the chemical potential difference. However, the activity coefficients estimated with this theory may have large errors when ionic species or highly acidic solutions are involved.[11] Despite the fact that many species will only be present in the dilute limit, the activity coefficients will not necessarily be close to one. This is because the actual system is concentrated nitric acid, whereas the reference state refers to

conditions when the solvent is pure water. The chemical potential of the solute will change when the solvent is changed from pure water to aqueous nitric acid, even when the solute is dilute; this is discussed in more detail in the Supporting Information. However, there currently does not appear to be any reliable way to accurately estimate the activity coefficients of the intermediates and transition states in nitric acid a priori. Some experimental activity coefficient data are available for the major species $HONO_2$, NO_3^-, H_3O^+, and H_2O and are discussed later in the paper.

$$k_{TST} = \kappa \frac{k_B T}{h} \left(\frac{\frac{Q_{TS}^o}{V_{TS}^o}}{\frac{Q_A^o}{V_A^o} \frac{Q_B^o}{V_B^o}} \right)_{gas} \times$$

$$\exp\left(\frac{-\Delta(E_{gas}^{0K} + \Delta G_{solv,ES}^* + \Delta G_{solv,non-ES}^*)_{TS}}{RT} \right) \quad (7)$$

In this work, the activity coefficients were neglected when determining rate coefficients because there is not a reliable method for calculating them for all species and transition states in solution; however, they are potentially very important to system behavior and continued work in this area could greatly benefit solution-phase modeling efforts. The TST rate coefficient was computed using eq 7, where $\Delta(E_{gas}^{0K} + \Delta G_{solv,ES}^* + \Delta G_{solv,non-ES}^*)_{TS}$ is the difference between the transition state energy and the reactant energies. When Gaussian is used, this is a natural way to formulate the problem because the 0 K energy returned in the thermochemistry section of a frequency calculation is the sum of the electronic energy, zero point energy, and electrostatic (ES) solvation free energy. The nonelectrostatic (non-ES) solvation free energy was also included in all TST calculations in this work. The solvation energy was taken to be constant when deriving the rate coefficient expressions as a function of temperature, which is a significant simplification. This assumption was made because it is difficult to estimate the temperature dependence of the solvation energy; however, recent research has shown that parametrized solvation models such as SM6T may provide a way to take these higher-order effects into account.[22,23] The partition functions were evaluated using traditional rigid-rotor/harmonic oscillator statistical mechanical expressions for the gas phase, leaving the solvation energies to account for all changes in the energetics and partition functions of the molecules when solvated. The rate coefficient expression was evaluated at temperatures between 273 and 403 K, and a modified Arrhenius form was fit to gain a simple expression for $k_{TST}(T)$ needed when solving the dynamic modeling equations.

Electron-Transfer Reactions. Electron-transfer reaction rates were estimated using Marcus Theory, with energetic parameters taken from computational chemistry calculations. Energies were calculated using the CBS-QB3 compound method with the IEFPCM solvation model and UAHF radii set. The simple version of Marcus Theory used here assumes a parabolic potential surface along the reaction coordinate for the reactant and product.[24-27] The reactant energy is zero at a reaction coordinate value of zero, and the product energy is ΔG_{rxn}^o at a reaction coordinate of one. The two surfaces will intersect, with the energy at this intersection being the approximate reaction barrier. The curvature of the reactant surface is estimated by performing an energy calculation for the each reactant molecule at the optimized reactant structure and one at the optimized structure of the product (e.g., the NO_2 energy would be

calculated at the NO_2 optimized geometry and the NO_2^- optimized geometry). The product surface is estimated in an analogous manner.

$$A + B \underset{}{\overset{K_C}{\rightleftharpoons}} A \cdots B \xrightarrow{k_{ET}} A^+ \cdots B^- \xrightarrow{fast} A^+ + B^- \quad (8)$$
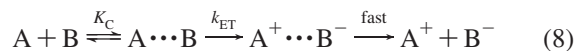
$$k_{overall,ET} = K_C k_{ET} \quad (9)$$

The rate coefficient was estimated assuming a three-step reaction process as shown in eq 8: diffusion to form an outer-sphere complex, electron transfer, and fast diffusion to free products. It was assumed that the enthalpy and nontranslational entropy of the outer-sphere complexes and the free reactants or products are equivalent because the species in either case would still be encased in separate solvent shells, shielding interactions between species. The translational entropy will differ because we are now forcing the two species to be within a certain distance from each other. The standard state translational entropy contribution is related to the volume accessible to the species (at standard state). The expression for K_C under ideal solution conditions is given in eq 10.

$$K_{C,ideal} = \frac{1}{C^o} \exp\left(\frac{1}{RT}[\Delta H^o - T\Delta S_{int} - T\Delta S_{trans}^o] \right) \quad (10)$$

$$K_{C,ideal} \approx \frac{1}{C^o} \frac{V_{free}^o}{V_{complex}} \quad (11)$$

With the enthalpy and internal entropy assumptions given earlier and relating the change in translational entropy to molecular volumes in the free and complexed states, we arrive at eq 11, where V_{free}^o is the standard state molecular volume of the free reactants, $V_{complex}$ is the molecular volume inside which the two reactant must exist to ensure an outer-sphere complex, and C^o is the standard state concentration (assumed to be the same for both reactants). If the standard state concentration is chosen to be 1 M, then the average molecule has an accessible volume equivalent to a 12 Å cube. At the standard state, one molecule of A and B will exist inside the same cube. If we assume that the center-to-center distance necessary to form an outer-sphere complex is ~10 Å (radii of 2 Å and water shell thicknesses of 3 Å each), then very little volume change is required to form the complex. In this fortuitous case, $K_{C,ideal} \approx 1 \, M^{-1}$ and $k_{overall,ET} \approx k_{ET} \cdot 1 \, M^{-1}$. The approximations made here are crude to be sure but are justified given the uncertainty present in other aspects of the simple Marcus Theory employed. However, understanding and accurately capturing these subtle details will be critical when more precise methodologies are developed.

The electron-transfer-rate coefficient was estimated using eq 12,[25] which employs a simplified pre-exponential factor and shows $\Delta G^\dagger$ as the free energy of activation for the electron transfer. The $\Delta G^\dagger$ term includes the electrostatic and nonelectrostatic solvation energies. More information on the methodology can be found in the Supporting Information.

$$k_{ET} = \frac{k_B T}{h} \exp\left(\frac{-\Delta G^\dagger}{RT} \right) \quad (12)$$

Reactions in Solvent Cages. The condensed phase can bring about new pathways and reactions types, one of which is a reaction in a solvent cage. Cage effects have been studied experimentally using the chemically induced dynamic nuclear polarization (CIDNP), mainly dealing with geminate radical recombination efficiency. We propose that cage effects play a major role in several of the reactions present in this mechanism,

particularly with "dissociative isomerizations in a solvent cage" (DISC). The two traditional ways in which an isomerization reaction proceeds are either though a concerted transition state or through a sequence where the reactant dissociates, the fragments diffuse apart, diffuse back together (geminate or not), and then reassociate in the isomeric form. The transition state pathway typically results in a higher reaction barrier but is unimolecular, whereas the dissociative pathway requires a bimolecular recombination. There is a tradeoff between the enthalpic and entropic changes with the two pathways, and it is not always clear which will dominate or if both are important.

In solution, we propose that this dissociative isomerization may happen completely within the solvent cage, preventing the two fragments from diffusing apart. The general reaction scheme is shown in eq 13. In this scenario, the fragmented complex is still considered a single species when the translational entropy is computed, because it occupies a single cavity in the solvent. Unlike the gas-phase dissociation-recombination isomerization sequence, this process can be treated unimolecularly and may achieve a faster rate of reaction. The main difficulty when estimating a rate coefficient for this type of reaction is computing the partition function or entropy of the poorly characterized caged complex. The way in which we choose to deal with this difficulty is through the use of the partition function in a manner similar to variational transition state theory (VTST). There are many incarnations of VTST with varying levels of complexity; we choose a relatively simply version presented by Forst as the basis of the caged rate coefficient estimates.[28,29]

$$\text{Reactant} \rightleftharpoons \overbrace{\left(Fragment\,\#1\cdots Fragment\,\#2\right)}^{caged\ complex} \rightleftharpoons \text{Product} \quad (13)$$
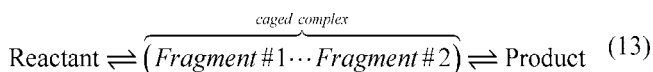
The need for VTST comes from several assumptions about our system. The first is that there may be a loose transition state between the reactant and the caged complex. Once the caged complex forms, it is assumed that the free energy surface is flat, and that all orientations of the fragments with respect to each other are equally likely. One further assumption made in this work is that the reaction coordinate is fully characterized by the distance between the fragments. To characterize this loose transition state, the potential energy surface and partition functions as a function of separation must be determined. These can be combined to yield the free energy surface of the reaction, from which the rate coefficient can be determined.

A partially constrained energy scan was performed using the MP2/6-31G(d′) level of theory and the IEFPCM solvation model with the UAHF radii set. The angle between the main chain in the larger fragment and the connected atom in the smaller fragment was held constant, e.g., the $H_2N-O-NO$ angle when NH_2ONO dissociates to NH_2O and NO radicals. All other degrees of freedom were optimized as the bond length was incremented. The energy profile including electrostatic and nonelectrostatic solvation energies, but excluding the zero point energy was obtained from this calculation. A frequency calculation was then performed at the same level of theory at each point along the trajectory, yielding vibrational and rotational frequencies. An additional rigid scan was performed as the reaction coordinate was increased, and one of the fragments was rotated in the plane of the reaction coordinate, e.g., the $H_2NO-N-O$ angle from 180° to 0°. This information was used to define the switching function discussed below, yielding insight into when the fragment interaction energy is small enough such that the fragments can rotate freely.

The transition of the partition function from the reactant molecule to the caged product complex can be handled in many ways; here we use a combination of a switching function and discrete calculations. The partition function contributions from the conserved and well defined degrees of freedom were calculated at each separation using the standard gas-phase treatment as used in Gaussian. The conserved modes corresponded to the vibrations that are present in the reactant and free fragments and the two overall rotational motions of the complex (the rotation about the centers of mass of the fragments is excluded). The partition function contribution from the two overall rotations was calculated as if the complex was a linear molecule. The overall rotation associated with the spinning about the axis connecting the centers of mass of the fragments is treated in a special manner, as described below. The unconserved vibrations were poorly behaved and often took on imaginary values as the fragment separation grew. One of these modes corresponds to the reaction coordinate. The rest are converted into the individual fragment rotations in the caged complex. To better understand the degree of freedom transfer, consider symmetric N_2O_4 breaking into two NO_2 radicals en route to forming $ONONO_2$. The reactant has 12 vibrations and 3 rotations. The two nonlinear NO_2 fragments each have 3 vibrations and 3 rotations, and the overall complex has 2 unique rotations, for a total of 14. The final degree of freedom is the reaction coordinate, matching the 15 of the reactant. The overall complex has only two unique rotations because the rotation about the axis connecting the centers of mass of the fragments is already accounted for by the individual fragments' rotations about this axis. The partition function contribution from the highest frequency rotational motion (about the centers of mass of the fragments) in the reactant molecule is transitioned from its value in the reactant to one at a large separation using the switching function to avoid double-counting this contribution in the caged complex.

The hyperbolic tangent switching function proposed by Forst was used to convert the unconserved vibrational partition function into the fragment rotational partition function, the single overall rotational mode discussed above, and the reactant zero point energy into the complex zero point energy. The zero point energy of the complex is simply taken to be the sum of zero point energies of the free fragments. The rotational partition function of the complex is taken to be the product of the rotational partition functions of the individual fragments and the contribution from the two overall rotational motions of the complex. The general form of the switching function is given in eq 14, where α and β are parameters describing the transfer, R is the separation, and R_{eq} is the equilibrium separation in the stable species. Typical gas-phase values are $0.05-0.15$ Å$^{-\beta}$ for α and usually near 2 for β.[29] Normally these parameters would be fit to experimental rate coefficient data to find best fit values, but another route had to be taken here because no experimental rate data was available for the desired rate coefficients.

$$S(R) = 1 - \tanh[\alpha(R - R_{eq})^{\beta}] \quad (14)$$

The rigid scan discussed earlier was used to estimate these parameters. The separation at which the fragments can freely rotate with respect to each other could be determined from the scan. The parameters of the switching function were set such that the value of the function was approximately 0.01 when the barrier to rotation dropped to less than k_BT. The exact parameter values for each reaction will be discussed later, but the values obtained in this manner appear reasonable given the typical range of the parameters.

$$\ln[Q(R)] = (\ln[Q_{react}] - \ln[Q_{complex}])S(R) + \ln[Q_{complex}] + \\ \ln[Q_{conserved}(R)] \quad (15)$$

Equation 15 was used to determine the total partition function at varying separation. The Q_{react} and $Q_{complex}$ partition function terms cover the unconserved modes and zero point energy in the reactant and complex that were transitioned using the switching function, whereas $Q_{conserved}$ accounts for all other degrees of freedom. Once the partition function has been computed as a function of separation, the free energy surface of the reaction can be calculated using eq 16. An estimate of the rate coefficient for complex formation is obtained using eq 17, where R_{TS} is the separation at which the free energy is the largest along the reaction path.

$$G(R) = E(R) + \Delta G_{solv}(R) - RT \ln[Q(R)] \quad (16)$$

$$k_{VTST} = \frac{k_B T}{h} \exp\left\{\frac{-[G(R_{TS}) - G(R_{eq})]}{RT}\right\} \quad (17)$$

Mechanism Development

The elementary reaction mechanism was developed starting from the previously published mechanisms discussed earlier. These mechanisms were broken down into elementary steps, and additional pathways were investigated and added (Table 2). One of the strengths of ab initio calculations is the ability to exclude certain reactions from the mechanism based on thermodynamic arguments. If the computed endothermicity of a reaction is extremely high, or significantly larger than a competing pathway, then the reaction may be safely excluded from the mechanism in most cases. A similar argument can be made using the TST estimates of the rate coefficients, but one must be more careful in this case because the TST estimates are more uncertain, and one cannot be confident that the lowest energy TS has been found. However, in some cases, rate coefficients estimates were used to eliminate certain reactions. The importance of individual reactions in the mechanism will be examined later when the modeling and sensitivity results are discussed.

The modeling was completed by assuming a constant volume, isothermal, closed system, as shown in eq 18, where $K_{C,m}$ is the appropriate equilibrium constant. The initial concentrations of nitric acid, hydroxylamine, and nitrous acid were changed to match the experimental conditions under which the data sets were collected, but a typical set was $[NH_2OH]_0 = 0.012$ M, $[HONO]_0 = 4 \times 10^{-5}$ M, $[HONO_2]_0 = 3$ M, $[O_2]_0 = 1 \times 10^{-4}$ M, $T = 298$ K, and the initial concentrations of all other species were set to zero. In some data sets, the initial concentration of the nitrate ion was nonzero due to the addition of a nitrate salt; these cases will be noted in the discussion.

$$\frac{dC_i}{dt} = \sum_{reactions,m} v_{i,m} k_{f,m} \left(\prod_{reacts,j} C_j^{v_{j,m}} - \frac{1}{K_{C,m}} \prod_{prods,j} C_j^{v_{j,m}}\right) \quad (18)$$
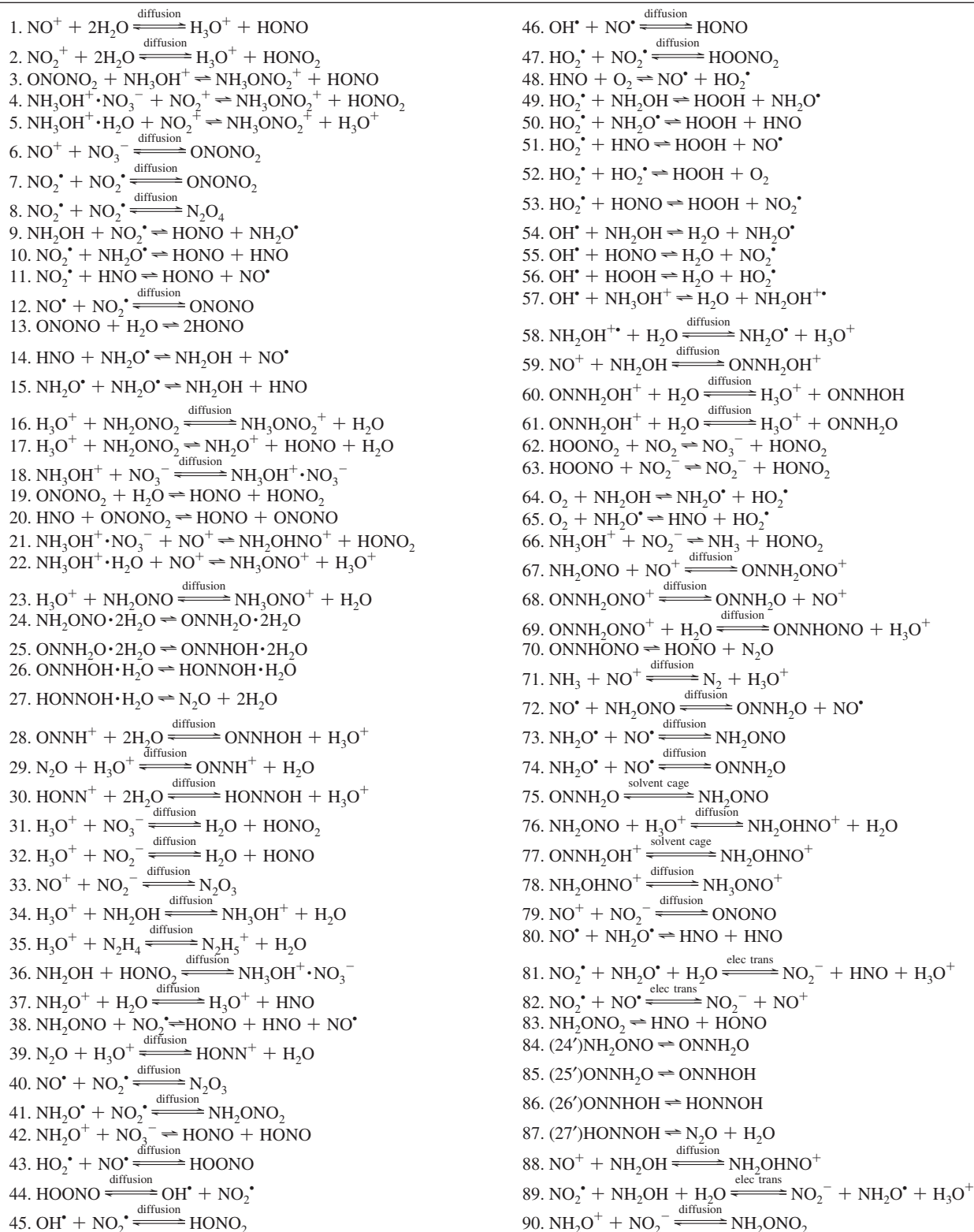
Results and Discussion

Rate Coefficient Estimates. *Transition State Theory.* Transition state structures for 41 reactions were investigated. A number of these reactions were examined in a previous work,[30] which neglected the effect of the nonelectrostatic solvation energy on the rate.[11] For several transition states and reactants, particularly those with explicit solvent molecules, we were not able to obtain a stationary point with the appropriate number of imaginary frequencies (one for a TS and zero for a stable

species). These specific cases will be addressed, and the reconciliation procedure will be described.

The solution-phase rate coefficient at 298 K, the magnitude of the imaginary frequency corresponding to the reaction coordinate, and the reaction barrier are shown in Table 3. Here the reaction barrier is defined as the sum of the 0 K electronic energy and the $\Delta\Delta G^*_{solv,TS}$ at 298 K, excluding the change in the free energy of cavitation ($\Delta\Delta G^*_{solv,cav}$). This term is excluded from the barrier because it is entropic in nature, and it is more appropriate to included it in the *A*-factor; although the rate coefficient at 298 K is not changed, it will affect the temperature dependence. Several reactions were computed to have negative barrier heights and were corrected to a diffusion-limit rate coefficient in the modeling work to ensure physical behavior.

Five of the 41 reactions listed in Table 3 required special treatment due to the presence of unwanted imaginary frequencies present in the reactant or transition state of a reaction; these reactions are indicated in Table 3 with a "c" superscript. The TS for reaction 5 contained an imaginary frequency of 31i cm^{-1} for the rotation of the approaching NO$_2$ group. This mode was treated as a free rotor when the TST rate coefficient was calculated and the frequency was removed. The reactant complex for reaction 24 had an imaginary frequency corresponding to a ring bending motion created by the complexed solvent molecules. A similar mode was observed in the transition state for reaction 24 with a frequency of 40 cm^{-1}, and the imaginary frequency of 44i cm^{-1} for the reactant was changed to match the transition state. A similar problem was observed for the reactant complex in reaction 25. An imaginary frequency of 23i cm^{-1} was changed to 25 cm^{-1} to match a similar motion seen in the transition state for reaction 24. The transition states for reactions 17 and 51 contained imaginary frequencies of 44i and 52i cm^{-1} for overall flexing of the TS structures, both of which were arbitrarily set to 100 cm^{-1}. We apologize for not being to rectify this numerical problem with very flat potential energy surfaces in a more rigorous scientific manner. Although the modifications to reactions 17 and 51 are arbitrary, it will be shown later that the overall reaction mechanism does not appear to be sensitive to either of these rate coefficients. The transition state for reaction 86 could not be successfully optimized at the B3LYP/CBSB7/IEFPCM level of theory. A single point PCM calculation was performed on the gas-phase-optimized transition state structure to estimate the solution-phase energy. The partition functions for this transition state were calculated using the vibrational and rotational frequencies for the gas-phase-optimized transition state geometry.

A limited amount of experimental solution-phase rate data is available for species present in this system. Bielski et al. have reviewed the reactivity of HO$_2$ in aqueous solution and have recommended a value for its self-reaction, represented by reaction 52 in our model.[31] They give the rate coefficient as $(8.3 \pm 0.7) \times 10^5$ L mol^{-1} s^{-1} for pH < 1.5, which is about one-fifth of our TST-estimated rate coefficient of 3.7×10^6 L mol^{-1} s^{-1}. Given the potential errors in the continuum solvation model and the potential pH dependence of the reaction, this represents reasonable agreement with the experimental data. Simic and Hayon have investigated the reaction of hydroxyl radical with protonated and unprotonated hydroxylamine.[32] They report the rate coefficient for reaction 54 (unprotonated) as 9.5×10^9 L mol^{-1} s^{-1} at a pH of 8 and for reaction 57 (protonated) as less than or equal to 5×10^8 L mol^{-1} s^{-1} at a pH of 4. Although there is a slight discrepancy between the experimental work, which list the NHOH radical as the product of reaction 54, and our computational chemistry work, which predicts NH$_2$O radical as the most probable product, the ab initio and

TABLE 2: Proposed Elementary Reaction Mechanism for the NH₂OH/HONO/HONO₂ System[a]

1. $NO^+ + 2H_2O \underset{}{\overset{\text{diffusion}}{\rightleftharpoons}} H_3O^+ + HONO$

2. $NO_2^+ + 2H_2O \underset{}{\overset{\text{diffusion}}{\rightleftharpoons}} H_3O^+ + HONO_2$

3. $ONONO_2 + NH_3OH^+ \rightleftharpoons NH_3ONO_2^+ + HONO$

4. $NH_3OH^+ \cdot NO_3^- + NO_2^+ \rightleftharpoons NH_3ONO_2^+ + HONO_2$

5. $NH_3OH^+ \cdot H_2O + NO_2^+ \rightleftharpoons NH_3ONO_2^+ + H_3O^+$

6. $NO^+ + NO_3^- \underset{}{\overset{\text{diffusion}}{\rightleftharpoons}} ONONO_2$

7. $NO_2^\bullet + NO_2^\bullet \underset{}{\overset{\text{diffusion}}{\rightleftharpoons}} ONONO_2$

8. $NO_2^\bullet + NO_2^\bullet \underset{}{\overset{\text{diffusion}}{\rightleftharpoons}} N_2O_4$

9. $NH_2OH + NO_2^\bullet \rightleftharpoons HONO + NH_2O^\bullet$

10. $NO_2^\bullet + NH_2O^\bullet \rightleftharpoons HONO + HNO$

11. $NO_2^\bullet + HNO \rightleftharpoons HONO + NO^\bullet$

12. $NO^\bullet + NO_2^\bullet \underset{}{\overset{\text{diffusion}}{\rightleftharpoons}} ONONO$

13. $ONONO + H_2O \rightleftharpoons 2HONO$

14. $HNO + NH_2O^\bullet \rightleftharpoons NH_2OH + NO^\bullet$

15. $NH_2O^\bullet + NH_2O^\bullet \rightleftharpoons NH_2OH + HNO$

16. $H_3O^+ + NH_2ONO_2 \underset{}{\overset{\text{diffusion}}{\rightleftharpoons}} NH_3ONO_2^+ + H_2O$

17. $H_3O^+ + NH_2ONO_2 \rightleftharpoons NH_2O^+ + HONO + H_2O$

18. $NH_3OH^+ + NO_3^- \underset{}{\overset{\text{diffusion}}{\rightleftharpoons}} NH_3OH^+ \cdot NO_3^-$

19. $ONONO_2 + H_2O \rightleftharpoons HONO + HONO_2$

20. $HNO + ONONO_2 \rightleftharpoons HONO + ONONO$

21. $NH_3OH^+ \cdot NO_3^- + NO^+ \rightleftharpoons NH_2OHNO^+ + HONO_2$

22. $NH_3OH^+ \cdot H_2O + NO^+ \rightleftharpoons NH_3ONO^+ + H_3O^+$

23. $H_3O^+ + NH_2ONO \underset{}{\overset{\text{diffusion}}{\rightleftharpoons}} NH_3ONO^+ + H_2O$

24. $NH_2ONO \cdot 2H_2O \rightleftharpoons ONNH_2O \cdot 2H_2O$

25. $ONNH_2O \cdot 2H_2O \rightleftharpoons ONNHOH \cdot 2H_2O$

26. $ONNHOH \cdot H_2O \rightleftharpoons HONNOH \cdot H_2O$

27. $HONNOH \cdot H_2O \rightleftharpoons N_2O + 2H_2O$

28. $ONNH^+ + 2H_2O \underset{}{\overset{\text{diffusion}}{\rightleftharpoons}} ONNHOH + H_3O^+$

29. $N_2O + H_3O^+ \underset{}{\overset{\text{diffusion}}{\rightleftharpoons}} ONNH^+ + H_2O$

30. $HONN^+ + 2H_2O \underset{}{\overset{\text{diffusion}}{\rightleftharpoons}} HONNOH + H_3O^+$

31. $H_3O^+ + NO_3^- \underset{}{\overset{\text{diffusion}}{\rightleftharpoons}} H_2O + HONO_2$

32. $H_3O^+ + NO_2^- \underset{}{\overset{\text{diffusion}}{\rightleftharpoons}} H_2O + HONO$

33. $NO^+ + NO_2^- \underset{}{\overset{\text{diffusion}}{\rightleftharpoons}} N_2O_3$

34. $H_3O^+ + NH_2OH \underset{}{\overset{\text{diffusion}}{\rightleftharpoons}} NH_3OH^+ + H_2O$

35. $H_3O^+ + N_2H_4 \underset{}{\overset{\text{diffusion}}{\rightleftharpoons}} N_2H_5^+ + H_2O$

36. $NH_2OH + HONO_2 \underset{}{\overset{\text{diffusion}}{\rightleftharpoons}} NH_3OH^+ \cdot NO_3^-$

37. $NH_2O^+ + H_2O \underset{}{\overset{\text{diffusion}}{\rightleftharpoons}} H_3O^+ + HNO$

38. $NH_2ONO + NO_2^\bullet \rightleftharpoons HONO + HNO + NO^\bullet$

39. $N_2O + H_3O^+ \underset{}{\overset{\text{diffusion}}{\rightleftharpoons}} HONN^+ + H_2O$

40. $NO^\bullet + NO_2^\bullet \underset{}{\overset{\text{diffusion}}{\rightleftharpoons}} N_2O_3$

41. $NH_2O^\bullet + NO_2^\bullet \underset{}{\overset{\text{diffusion}}{\rightleftharpoons}} NH_2ONO_2$

42. $NH_2O^+ + NO_3^- \rightleftharpoons HONO + HONO$

43. $HO_2^\bullet + NO^\bullet \underset{}{\overset{\text{diffusion}}{\rightleftharpoons}} HOONO$

44. $HOONO \underset{}{\overset{\text{diffusion}}{\rightleftharpoons}} OH^\bullet + NO_2^\bullet$

45. $OH^\bullet + NO_2^\bullet \underset{}{\overset{\text{diffusion}}{\rightleftharpoons}} HONO_2$

46. $OH^\bullet + NO^\bullet \underset{}{\overset{\text{diffusion}}{\rightleftharpoons}} HONO$

47. $HO_2^\bullet + NO_2^\bullet \underset{}{\overset{\text{diffusion}}{\rightleftharpoons}} HOONO_2$

48. $HNO + O_2 \rightleftharpoons NO^\bullet + HO_2^\bullet$

49. $HO_2^\bullet + NH_2OH \rightleftharpoons HOOH + NH_2O^\bullet$

50. $HO_2^\bullet + NH_2O^\bullet \rightleftharpoons HOOH + HNO$

51. $HO_2^\bullet + HNO \rightleftharpoons HOOH + NO^\bullet$

52. $HO_2^\bullet + HO_2^\bullet \rightleftharpoons HOOH + O_2$

53. $HO_2^\bullet + HONO \rightleftharpoons HOOH + NO_2^\bullet$

54. $OH^\bullet + NH_2OH \rightleftharpoons H_2O + NH_2O^\bullet$

55. $OH^\bullet + HONO \rightleftharpoons H_2O + NO_2^\bullet$

56. $OH^\bullet + HOOH \rightleftharpoons H_2O + HO_2^\bullet$

57. $OH^\bullet + NH_3OH^+ \rightleftharpoons H_2O + NH_2OH^{+\bullet}$

58. $NH_2OH^{+\bullet} + H_2O \underset{}{\overset{\text{diffusion}}{\rightleftharpoons}} NH_2O^\bullet + H_3O^+$

59. $NO^+ + NH_2OH \underset{}{\overset{\text{diffusion}}{\rightleftharpoons}} ONNH_2OH^+$

60. $ONNH_2OH^+ + H_2O \underset{}{\overset{\text{diffusion}}{\rightleftharpoons}} H_3O^+ + ONNHOH$

61. $ONNH_2OH^+ + H_2O \underset{}{\overset{\text{diffusion}}{\rightleftharpoons}} H_3O^+ + ONNH_2O$

62. $HOONO_2 + NO_2^- \rightleftharpoons NO_3^- + HONO_2$

63. $HOONO + NO_2^- \rightleftharpoons NO_2^- + HONO_2$

64. $O_2 + NH_2OH \rightleftharpoons NH_2O^\bullet + HO_2^\bullet$

65. $O_2 + NH_2O^\bullet \rightleftharpoons HNO + HO_2^\bullet$

66. $NH_3OH^+ + NO_2^- \rightleftharpoons NH_3 + HONO_2$

67. $NH_2ONO + NO^+ \underset{}{\overset{\text{diffusion}}{\rightleftharpoons}} ONNH_2ONO^+$

68. $ONNH_2ONO^+ \underset{}{\overset{\text{diffusion}}{\rightleftharpoons}} ONNH_2O + NO^+$

69. $ONNH_2ONO^+ + H_2O \underset{}{\overset{\text{diffusion}}{\rightleftharpoons}} ONNHONO + H_3O^+$

70. $ONNHONO \rightleftharpoons HONO + N_2O$

71. $NH_3 + NO^+ \underset{}{\overset{\text{diffusion}}{\rightleftharpoons}} N_2 + H_3O^+$

72. $NO^\bullet + NH_2ONO \underset{}{\overset{\text{diffusion}}{\rightleftharpoons}} ONNH_2O + NO^\bullet$

73. $NH_2O^\bullet + NO^\bullet \underset{}{\overset{\text{diffusion}}{\rightleftharpoons}} NH_2ONO$

74. $NH_2O^\bullet + NO^\bullet \underset{}{\overset{\text{diffusion}}{\rightleftharpoons}} ONNH_2O$

75. $ONNH_2O \underset{}{\overset{\text{solvent cage}}{\rightleftharpoons}} NH_2ONO$

76. $NH_2ONO + H_3O^+ \underset{}{\overset{\text{diffusion}}{\rightleftharpoons}} NH_2OHNO^+ + H_2O$

77. $ONNH_2OH^+ \underset{}{\overset{\text{solvent cage}}{\rightleftharpoons}} NH_2OHNO^+$

78. $NH_2OHNO^+ \underset{}{\overset{\text{diffusion}}{\rightleftharpoons}} NH_3ONO^+$

79. $NO^+ + NO_2^- \underset{}{\overset{\text{diffusion}}{\rightleftharpoons}} ONONO$

80. $NO^\bullet + NH_2O^\bullet \rightleftharpoons HNO + HNO$

81. $NO_2^\bullet + NH_2O^\bullet + H_2O \underset{}{\overset{\text{elec trans}}{\rightleftharpoons}} NO_2^- + HNO + H_3O^+$

82. $NO_2^\bullet + NO^\bullet \underset{}{\overset{\text{elec trans}}{\rightleftharpoons}} NO_2^- + NO^+$

83. $NH_2ONO_2 \rightleftharpoons HNO + HONO$

84. $(24')NH_2ONO \rightleftharpoons ONNH_2O$

85. $(25')ONNH_2O \rightleftharpoons ONNHOH$

86. $(26')ONNHOH \rightleftharpoons HONNOH$

87. $(27')HONNOH \rightleftharpoons N_2O + H_2O$

88. $NO^+ + NH_2OH \underset{}{\overset{\text{diffusion}}{\rightleftharpoons}} NH_2OHNO^+$

89. $NO_2^\bullet + NH_2OH + H_2O \underset{}{\overset{\text{elec trans}}{\rightleftharpoons}} NO_2^- + NH_2O^\bullet + H_3O^+$

90. $NH_2O^+ + NO_2^- \underset{}{\overset{\text{diffusion}}{\rightleftharpoons}} NH_2ONO_2$

[a] Diffusion-limited, electron transfer, and solvent-cage reactions are specified; others estimated via TST.

experimental results agree to within an order of magnitude. Both rate coefficients are essentially at the diffusion limit in solution. The rate of abstraction from NH_3OH^+ by OH was found to be diffusion limited, given that the TST barrier was estimated to be large and negative, yielding an aphysical rate coefficient.

Many of the reactions are analogous to what occurs in the gas phase, such as H-abstractions, radical recombination, radical disproportionation, and concerted reactions between stable,

closed-shell molecules. Because these reactions types have been studied in detail in many other places, here we simply report the reaction parameters and rate coefficient estimates in aqueous solution. Attention will be focused on less understood reactions, such as those where explicit solvent molecules play a role and reactions involving ionic species.

Reactions with explicit solvent molecules are particularly interesting because they are usually unique to condensed-phase

TABLE 3: Transition State Theory Rate Coefficient Estimates in Solution at 298 K[a]

	reaction	k(298K) (mol L s)	$\nu_{imaginary}$ (cm^{-1})	barrier (kcal/mol)
3	$ONONO_2 + NH_3OH^+ \rightleftharpoons NH_3ONO_2^+ + HONO$	2.5E−17	735	33.2[b]
4	$NH_3OH^+ \cdot NO_3^- + NO_2^+ \rightleftharpoons NH_3ONO_2^+ + HONO_2$	7.3E+07	821	0.9[b]
5	$NH_3OH^+ \cdot H_2O + NO^{2+} \rightleftharpoons NH_3ONO_2^+ + H_3O^+$	3.2E+01	347	10.9[b,c]
9	$NH_2OH + NO_2 \rightleftharpoons HONO + NH_2O$	3.4E+03	601	6.2[b]
10	$NO_2 + NH_2O \rightleftharpoons HONO + HNO$	3.9E+00	632	9.1[b]
11	$NO_2 + HNO \rightleftharpoons HONO + NO$	1.2E+02	1064	9.5[b]
13	$ONONO + H_2O \rightleftharpoons 2HONO$	3.5E+04	1012	6.0[b]
14	$HNO + NH_2O \rightleftharpoons NH_2OH + NO$	8.4E+05	1549	5.0
15	$NH_2O + NH_2O \rightleftharpoons NH_2OH + HNO$	7.8E−03	981	13.1
17	$H_3O^+ + NH_2ONO_2 \rightleftharpoons NH_2O^+ + HONO + H_2O$	1.6E−13	187	26.7[b,c]
19	$ONONO_2 + H_2O \rightleftharpoons HONO + HONO_2$	1.4E+08	756	0.7[b]
20	$HNO + ONONO_2 \rightleftharpoons HONO + ONONO$	5.3E+06	474	0.7[b]
21	$NH_3OH^+ \cdot NO_3^- + NO^+ \rightleftharpoons NH_2OHNO^+ + HONO_2$	4.4E+10	867	−2.9[b,d]
22	$NH_3OH^+ \cdot H_2O + NO^+ \rightleftharpoons NH_3ONO^+ + H_3O^+$	1.7E+06	333	2.9[b]
24	$NH_2ONO \cdot 2H_2O \rightleftharpoons ONNH_2O \cdot 2H_2O$	9.0E+02	193	13.3[b,c]
25	$ONNH_2O \cdot 2H_2O \rightleftharpoons ONNHOH \cdot 2H_2O$	9.5E+07	1083	7.1[b,c]
26	$ONNHOH \cdot H_2O \rightleftharpoons HONNOH \cdot H_2O$	7.6E+04	1118	10.5
27	$HONNOH \cdot H_2O \rightleftharpoons N_2O + 2H_2O$	1.4E−01	765	17.6
38	$NH_2ONO + NO_2 \rightleftharpoons HONO + HNO + NO$	2.3E−04	242	16.1[b]
48	$HNO + O_2 \rightleftharpoons NO + HO_2$	7.7E+02	1624	10.5
49	$HO_2 + NH_2OH \rightleftharpoons HOOH + NH_2O$	6.8E+05	854	3.9
50	$HO_2 + NH_2O \rightleftharpoons HOOH + HNO$	8.0E+00	865	9.5
51	$HO_2 + HNO \rightleftharpoons HOOH + NO$	4.0E+07	200	1.6[c]
52	$HO_2 + HO_2 \rightleftharpoons HOOH + O_2$	3.7E+06	536	2.5
53	$HO_2 + HONO \rightleftharpoons HOOH + NO_2$	8.8E−02	1974	14.8
54	$OH + NH_2OH \rightleftharpoons H_2O + NH_2O$	8.2E+10	945	−1.5[d]
55	$OH + HONO \rightleftharpoons H_2O + NO_2$	1.9E+06	1574	5.3
56	$OH + HOOH \rightleftharpoons H_2O + HO_2$	3.6E+09	294	0.4
57	$OH + NH_3OH^+ \rightleftharpoons H_2O + NH_2OH^+$	2.3E+28	1547	−24.7[d]
62	$HOONO_2 + NO_2^- \rightleftharpoons NO_3^- + HONO_2$	3.3E+04	440	4.1
63	$HOONO + NO_2^- \rightleftharpoons NO_2^- + HONO_2$	4.5E+05	410	3.9
64	$O_2 + NH_2OH \rightleftharpoons NH_2O + HO_2$	6.0E−02	1354	15.5
65	$O_2 + NH_2O \rightleftharpoons HNO + HO_2$	1.3E−05	1886	21.0
66	$NH_3OH^+ + NO_2^- \rightleftharpoons NH_3 + HONO_2$	7.0E−04	433	15.3
70	$ONNHONO \rightleftharpoons HONO + N_2O$	8.1E+00	852	17.1
80	$NO + NH_2O \rightleftharpoons HNO + HNO$	1.4E−13	852	29.7
83	$NH_2ONO_2 \cdot H_2O \rightleftharpoons HNO + HONO + H_2O$	1.2E+00	1037	16.9
84	(24′) $NH_2ONO \rightleftharpoons ONNH_2O$	1.6E−02	199	19.5[b]
85	(25′) $ONNH_2O \rightleftharpoons ONNHOH$	4.2E−14	1669	37.2[b]
86	(26′) $ONNHOH \rightleftharpoons HONNOH$	3.2E−10	1778	31.9[b,c]
87	(27′) $HONNOH \rightleftharpoons N_2O + H_2O$	6.9E−01	1207	18.3[b]

[a] Unimolecular rate coefficients in s^{-1}; bimolecular rate coefficients in L mol^{-1} s^{-1}. [b] Calculated in current work; also examined in a previous work by Raman et al.[30] [c] Nonstandard treatment required; see text for details. [d] Negative reaction barrier; corrected to be diffusion-limited in the modeling work.

systems. In the protic solvent examined here, solvent molecules serve as proton acceptors, assist in intramolecular hydrogen transfers, or may help to stabilize transition state structures. In reactions examined using transition state theory, water served as a proton acceptor in reactions 5, 17, and 22. Reactions 5 and 22 are very similar in that they both involve a positive ion attacking the oxygen lone pair in NH_3OH^+. A proton acceptor is necessary because doubly charged ionic species would be very unfavorable. Allowing the simultaneous loss of a proton to the solvent yields a low energy transition state and product, creating a potentially favorable reaction. In these cases, the positively charged electrophile begins to bond to the O atom, which simultaneously loses a proton to a hydrogen-bonded water molecule. Reaction 17 is another example of when a high-energy intermediate would be formed if a proton acceptor was not immediately available.

Reactions where water molecules serve as a hydrogen-transfer agents are also common, as can be seen in reactions 25−27 and 83. In these cases, the traditional transition states without explicit solvent molecules (as in reactions 85−87) contain highly strained ring structures necessary to transfer the hydrogen from one position in the molecule to another. The result is usually a high energetic barrier to the reaction. The inclusion of the solvent molecule(s) allows the ring structure to be larger and less strained, causing the transition state energy to be lower, when compared to small, cyclic transition state structures. Here, one (or more) water molecule simultaneously accepts a hydrogen atom at a lone pair site and gives up one of its original hydrogen atoms to another molecule. A comparison of the barriers is shown in Table 4 for reactions 25−27 and their unassisted counterparts, 85−87. Reaction 85 is an α-β hydrogen transfer, where the hydrogen shifts from one atom to its direct neighbor, creating a three-membered ring in the transition state, including the hydrogen atom. Reaction 86 is an α-γ hydrogen transfer, creating a four-membered ring in the transition state, and reaction 87 is an α-δ hydrogen transfer, creating a 5-membered ring.

The benefit provided by the explicit solvent molecules is clear, especially with small, strained ring structures. The inclusion of two water molecules in reaction 25 results in a 30 kcal/mol decrease in the reaction barrier. Reaction 26 sees a decrease of over 20 kcal/mol with the addition of a single solvent molecule. The benefit to reaction 27 is small, and likely not significant given the uncertainty present in the computation method. There

Oxidation of Hydroxylamine by Aqueous Nitric Acid

J. Phys. Chem. A, Vol. 112, No. 33, 2008 **7585**

TABLE 4: Comparison of Water-Assisted and Unassisted Intramolecular H-transfer Reactions

	reaction	barrier (kcal/mol)	ν_{imag} (cm^{-1})	k(298K) (mol L s)
25	ONNH$_2$O·2H$_2$O $\rightleftharpoons$ ONNHOH·2H$_2$O	7.1	1083	9.5E+07
85	ONNH$_2$O $\rightleftharpoons$ ONNHOH	37.2	1669	4.2E−14
26	ONNHOH·2H$_2$O $\rightleftharpoons$ HONNOH·H$_2$O	10.5	1118	7.6E+04
86	ONNHOH $\rightleftharpoons$ HONNOH	31.9	1778	3.2E−10
27	HONNOH·H$_2$O $\rightleftharpoons$ N$_2$O + 2H$_2$O	17.6	765	1.4E−01
87	HONNOH $\rightleftharpoons$ N$_2$O + H$_2$O	18.3	1207	6.9E−01

are two reasons for this: the five-membered transition state ring is not highly strained and/or the barrier is dominated by the energy required to sever the N−O bond. The most important point here is that some reactions change from completely unfavorable without solvent molecules to fast and potentially significant with explicit solvent molecules.

Explicit water molecules were also included in reaction 24 because it was seen to reduce the barrier; even through the solvent molecules do not significantly affect the motion along the reaction coordinate. Despite the lack of a direct role in the reaction, the two hydrogen-bonded solvent molecules reduce the barrier from a value of 20 kcal/mol to 13 kcal/mol. It is unusual to see such a large barrier reduction; a more comprehensive study would be helpful to elucidate the origin of this effect.

Another interesting set of reactions modeled using transition state theory were those of peroxynitrous and peroxynitric acid. These species mainly arise out of the reactions involving dissolved oxygen following the formation of HO$_2$ or OH radicals, which subsequently react with NO or NO$_2$ radicals to form peroxides. The peroxides can then react with the nitrite ions in solution, as shown in reactions 62 and 63. The reaction of peroxynitrous acid (HOONO) with nitrite has been studied previously by Maurer et al.[33] The authors concluded that the HO$^+$ transfer from the peroxy species to the nitrite ion is the predominant mechanism by which the reaction occurs. Mauer et al. also give a "Helmholtz" activation barrier of 1.5 ± 2.9 kcal/mol based on ab initio molecular dynamics calculations with species concentrations equivalent to ∼1 M. The zero-point corrected potential energy barrier computed in the present work by the ab initio PCM method was 3.1 kcal/mol, similar to the barrier of Maurer. We compare the PCM potential energy barrier to the "Helmholtz" barrier because Mauer states that the two fragments treated as the reactant in their study are not far enough apart to be independently solvated; i.e., there is not a large entropy change between the "reactants" (nonisolated) and transition state in the MD simulation. This makes the Helmholtz energy barrier in the MD simulation similar to a potential energy barrier. The net result of this reaction is the isomerization of peroxynitrous acid to nitric acid, catalyzed by a nitrite ion. The reaction of peroxynitric acid (HOONO$_2$) also proceeds via OH$^+$ transfer, but with the product being a nitric acid molecule and nitrate ion.

Three additional rate coefficients in the system had experimentally derived measurements available. Reaction 22 was reported to be 6 × 10^6 M^{-1} s^{-1} at 298 K by Bourke and Stedman, though the validity of this estimate is questionable because of the pseudosteady state approximation used to derive it.[14] The TST estimate of 1.7 × 10^6 M^{-1} s^{-1} is quite close to the experimental value. The rate coefficient for reaction 13 was cited to be 10 M^{-1} s^{-1} at 293 K and 37 M^{-1} s^{-1} at 298 K, and the rate coefficient for reaction 19 was said to be ∼15 M^{-1} s^{-1} by Schwartz and White.[34] These results disagree with our calculated values; however, the TST estimates are based on the higher energy reactant isomers (ONONO$_2$ and ONONO)

whereas the rate coefficients inferred by Schwartz and White imply the more stable symmetric N$_2$O$_4$ and asymmetric N$_2$O$_3$ as the reactants. Combine this with the fact that these reactions make little difference in the HONO yield or ignition time, and we can ignore this discrepancy with little concern to overall system behavior.

We briefly examined the effect of quantum chemistry method employed on the computed reaction barriers, comparing the B3LYP results discussed above with MP2 calculations. Five reactions were studied (19, 26, 63, 80, and 84). These reactions represent a good range of the reaction types included in the mechanism. No clear trends were observed. The only conclusion that can be drawn from this is that there are some discrepancies between B3LYP and MP2 barrier heights, with the main differences appearing in the electronic and electrostatic solvation energies, as would be expected. More information can be found in the Supporting Information.

Electron Transfer. Three reactions, shown below, were modeled using simple Marcus theory to estimate the rate coefficient. The reactions whose direct electron-transfer product contains a labile proton (NH$_2$O$^+$ in reaction 81 and NH$_2$OH$^+$ in reaction 89) were modeled both with and without an explicit water molecule to accept the proton. After the electron is transferred (or perhaps simultaneously), the proton will spontaneously move to the explicit water molecule, forming H$_3$O$^+$ complexed to a neutral product. When the reactions are modeled without an explicit water molecule, the N−H or O−H bond distances in the product ion (∼1.08 Å) are significantly larger than in reactant (0.98−1.02 Å), but still quite close to the parent. A major difference between these two approaches was seen to be the reorganization energy. This energy depends on the structural differences between the reactant and product, which are more pronounced with the explicit water molecule present than without. These calculations are fraught with uncertainty stemming from the ambiguity in defining the "true" reaction, differences in energetics as the level of theory is changed (particularly in the nonequilibrium structures), and general assumptions built into the simple Marcus theory. That being said, this analysis should provide a reasonable first estimate of the electron-transfer rates.

$$81. \quad NO_2^{\bullet} + NH_2O^{\bullet} + H_2O \overset{\text{elec trans}}{\rightleftharpoons} NO_2^- + HNO + H_3O^+$$

$$82. \quad NO_2^{\bullet} + NO^{\bullet} \overset{\text{elec trans}}{\rightleftharpoons} NO_2^- + NO^+$$

$$89. \quad NO_2^{\bullet} + NH_2OH + H_2O \overset{\text{elec trans}}{\rightleftharpoons} NO_2^- + NH_2O^{\bullet} + H_3O^+$$
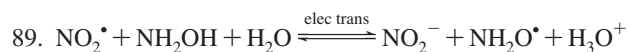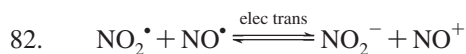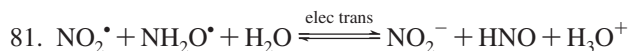
Reaction 82 was the simplest because no hydrogen atoms are involved, eliminating the need to consider explicit solvent molecules. The reorganization energies were found to be small, which was expected given that the reactant and product structures are quite similar. The A_R and A_P terms are the force
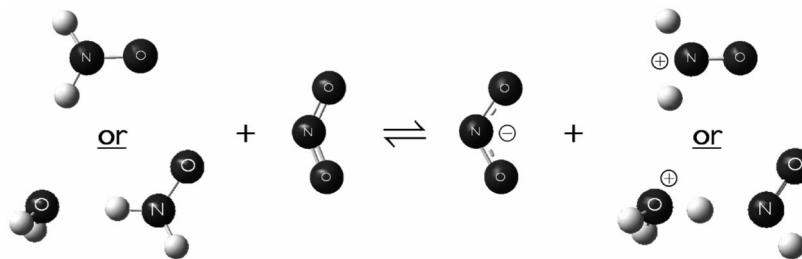
Figure 1. Reaction 81 electron-transfer geometries with and without an explicit water molecule.
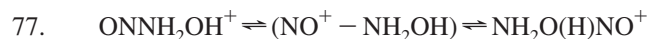
constants of the 1-D parabolic energy surfaces of the reactant and product along the assumed reaction coordinate. As written, A_R and A_P were determined to be 28.6 and 29.6 kcal/mol, respectively, of which 15−20 kcal/mol is attributed to NO_2 or NO_2^- reorganization. The energy change for the reaction based on solution-phase CBS-QB3 calculations was 17 kcal/mol, compared with ∼10 kcal/mol with the semiempirical method described in the Thermochemistry section. Regardless of which energy of reaction is used, the reverse of reaction 82 is predicted to have a barrier of 1−3 kcal/mol, which corresponds to a diffusion-limited reaction. In the models to be discussed later, this reaction was taken to be diffusion-limited in the exothermic (i.e., reverse) direction.

Reaction 81 is complicated somewhat by the labile proton, so the analysis was completed with and without an explicit solvent molecule. The species' geometries are shown in Figure 1 for both cases; note the significant structural differences in the two situations. Without an explicit water molecule, the A_R and A_P were determined to be 26.2 and 28.4 kcal/mol, with an energy change of reaction of 11 kcal/mol. This translates into a barrier of 13.3 kcal/mol and a rate coefficient of 1.1×10^3 M^{-1} s^{-1} at 298 K. With the explicit water molecule, A_R and A_P were 61.1 and 40.78 kcal/mol, with an energy change of reaction of 0.2 kcal/mol. This yields a barrier of 12.5 kcal/mol and a rate coefficient of 4.1×10^3 M^{-1} s^{-1} at 298 K. The close agreement of the barriers with and without a solvent molecule is likely coincidental, because we will show very different results for reaction 89. Empirical corrections to the thermochemistry decrease the energy of reaction by ∼2 kcal/mol, resulting in a barrier of ∼11.5 kcal/mol and a rate coefficient that is an order of magnitude faster. Taking this into account, a reasonable estimate of the barrier and rate coefficient would be 12 ± 3 kcal/mol and 1×10^4 M^{-1} s^{-1}, respectively. Note that this ultimately results in the same products and is several orders of magnitude faster than the direct H-abstraction (reaction 10).

Reaction 89 was treated in an analogous manner to 81. A large difference was again seen in the reorganization energies with and without the solvent molecule. Without an explicit water molecule, the A_R and A_P were determined to be 46.6 and 58.0 kcal/mol, with an energy change of reaction of 6.8 kcal/mol, resulting in a barrier of 16.4 kcal/mol and a rate coefficient of 5.6 M^{-1} s^{-1} at 298 K. With the explicit water molecule, A_R and A_P were 72.0 and 67.3 kcal/mol, with an energy change of reaction of 5.9 kcal/mol. This yields a barrier of 20.5 kcal/mol and a rate coefficient of 5.5×10^{-3} M^{-1} s^{-1} at 298 K. Either way, this electron transfer appears to not be competitive with the direct H-abstraction (reaction 9) that has a rate coefficient on the order of 10^3 M^{-1} s^{-1}. As discussed below, the model predictions are sensitive to the rate of reaction 9 and its alternative, reaction 89. If the simple Marcus theory estimate of the barrier for reaction 89 is flawed and the electron transfer actually proceeds significantly faster than the H-abstraction, it would have a major impact on the dynamics of the system.

To test the validity of the electron-transfer rate estimation approach used here, we computationally examined the reaction of CH_2OH radical with NO_2 and compared the results with the experimentally derived rate coefficient of 1×10^9 M^{-1} s^{-1}.[35] We only considered the case with an explicit water molecule present in the calculations but examined the reaction at the B3LYP/CBSB7 and CBS-QB3 levels of theory with the same IEFPCM solvation model used throughout. For the B3LYP/CBSB7 case, A_R and A_P were 60.6 and 53.3 kcal/mol, with an energy change of reaction of −22.9 kcal/mol due to the favorability of formaldehyde formation. This yields a barrier of 4.7 kcal/mol and a rate coefficient of 2.1×10^9 M^{-1} s^{-1} at 298 K. At the CBS-QB3 level, A_R and A_P were 57.9 and 47.7 kcal/mol, with an energy change of reaction of −35.6 kcal/mol, resulting in a barrier of 0.5 kcal/mol and a diffusion-limited rate coefficient. These results agree well with the experimental finding that this electron-transfer reaction is nearly diffusion limited, primarily due to the large exothermicity of the reaction.

Solvent Cage Reactions. Reactions 75 and 77 were treated as dissociative isomerizations in a solvent cage. These reactions are not only important to the scavenging pathway that converts hydroxylamine to nitrous oxide but also may have a significant impact on the branching ratio between the scavenging and autocatalytic pathways. The two traditional isomerization pathways for reaction 75 are present in the mechanism in the forms of reaction 24, reaction 84, and the combination of reactions 73 and 74. A direct isomerization transition state was not found for reaction 77, but the fully dissociative isomerization pathway is included with reactions 59 and 88.

75r. $\quad NH_2ONO \rightleftharpoons (NO^\bullet - NH_2O^\bullet) \rightleftharpoons ONNH_2O$

77. $\quad ONNH_2OH^+ \rightleftharpoons (NO^+ - NH_2OH) \rightleftharpoons NH_2O(H)NO^+$

Determining the potential energy surface for the dissociation of NH_2ONO requires multiple calculations because the singlet state is most stable at small separations, whereas the triplet (two radical fragments) is most stable at large separations. The restricted singlet state at large separations corresponds to ionic species NH_2O^- and NO^+, which are much less stable than their radical counterparts. For this reaction, a constrained scan was performed for the restricted singlet and restricted triple states. The singlet energies were taken when $R - R_{eq} < 1.25$ Å (the approximate point at which the restricted singlet and triplet energy surfaces cross), and triplet energies were used at larger separations. The equilibrium N−O separation was $R_{eq} = 1.45$ Å. The composite surface was used in the calculation of the rate coefficient and can be seen below in Figure 2. A rigid scan showed that the barrier to rotation of the NO fragment was less than k_BT when the N−O distance was larger than 4.5 Å, or $R - R_{eq} > 3.0$ Å. The parameters chosen for the switching function for this reaction were $\alpha = 0.15$ Å$^{-2.5}$ and $\beta = 2.5$, allowing $S(R)$ to achieve a value of 0.015 at an N−O distance of 4.5 Å. The values of the partition function contributions as a function of separation are presented in the Supporting Information.
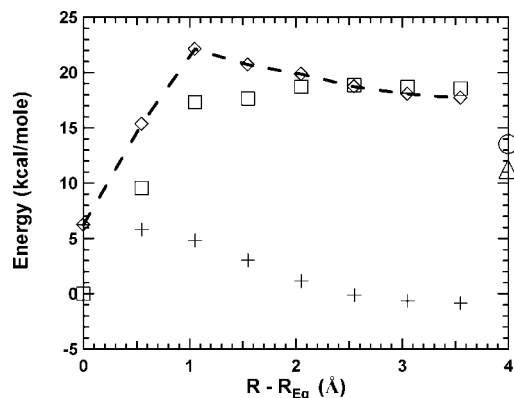
Oxidation of Hydroxylamine by Aqueous Nitric Acid

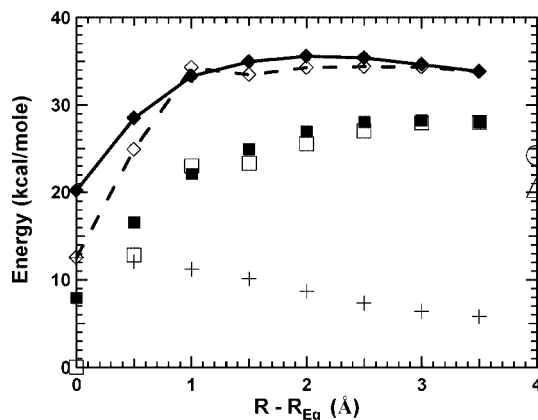*J. Phys. Chem. A, Vol. 112, No. 33, 2008* **7587**

Figure 2. Potential energy ($\square$) and free energy ($\diamond$ and dashed line) surfaces for the dissociation of NH_2ONO (reaction 75); partition function and ZPE contribution to free energy (+); $ONNH_2O$ free energy ($\triangle$); dissociated fragments free energy ($\bigcirc$). All at 298 K and a standard state concentration of 0.0409 M.

Figure 3. Potential energy ($\square$) and free energy ($\diamond$ and dashed line) surfaces for the dissociation of $ONNH_2OH^+$ (reaction 77); partition function and ZPE contribution to free energy for $ONNH_2OH^+$ (+); potential energy ($\blacksquare$) and free energy ($\blacklozenge$ and solid line) surfaces for the dissociation of NH_2OHNO^+ relative to $ONNH_2OH^+$; NH_2OHNO^+ free energy ($\triangle$); dissociated fragment free energy ($\bigcirc$). All at 298 K and a standard state concentration of 0.0409 M.

The partition function and the potential energy, including electrostatic and nonelectrostatic solvation energies, can be combined to yield the free energy along the reaction coordinate, as was shown in eq 16. The free energy profile is given in Figure 2 along with the total partition function contribution to the free energy ($-RT \ln[Q_{total}]$), including the zero point energy. A transition state can clearly be seen from the free energy profile and is located at a separation of 2.5 Å, or $R - R_{eq} \approx 1.0$ Å. The free energy change from the reactant to transition state (ΔG_{TS}) is 15.9 kcal/mol. Using this value with eq 17 yields a rate coefficient estimate of 1.3×10^1 s^{-1} for the formation of the caged complex from NH_2ONO. It appears that the free energy surface flattens out after the transition state, so we estimate the free energy change from the reactant to the complex to be $\sim$11.5 kcal/mol. The nonelectrostatic solvation free energy accounts for $\sim$1.7 kcal/mol of the free energy barrier. The translation of the free energy surface into a rate coefficient for the overall caged isomerization reaction is discussed below. The free energy of $ONNH_2O$ (11.2 kcal/mol) and free fragments (13.5 kcal/mol) relative to the NH_2ONO potential energy are also shown in Figure 2 for a standard state concentration of 0.0409 M at 298 K.

The characterization of reaction 77 was more straightforward because the reactant and complex were always most stable in the singlet electronic state. The energy, free energy, and partition function contribution to free energy are shown in Figure 3, and a summary of the partition function with separation is given in the Supporting Information. For this reaction, we also include the potential and free energy profile for the isomerization product breaking at the O−N bond. The energy profiles for both reactant and product are very similar, as is the barrier to convert the complex to either $ONNH_2OH^+$ or NH_2OHNO^+. The partition function contribution to the free energy is essentially identical for the reactant and product, so only that of $ONNH_2OH^+$ is shown here. A rigid scan revealed that the NO^+ fragment could rotate freely with respect to the NH_2OH fragment when $R - R_{eq} > 4.0$ Å. The equilibrium separation was 1.92 Å in $ONNH_2OH^+$ and 2.14 Å in NH_2OHNO^+. The parameters used in the switching function for both the reactant and product were $\alpha = 0.15$ Å^{-2} and $\beta = 2$, allowing $S(R)$ to achieve a value of 0.016 when $R - R_{eq} = 4.0$ Å. The free energy barrier for this reaction was determined to be 21.7 kcal/mol, resulting in a rate coefficient estimate of 7.5×10^{-4} s^{-1} for the reaction of $ONNH_2OH^+$ to the caged complex. The nonelectrostatic solvation free energy accounts for $\sim$1.6 kcal/mol of the barrier in

this reaction. The free energy change from the reactant to the complex is $\sim$21.2 kcal/mol for this reaction.

Figure 4 provides a summary of the free energy surfaces for reactions 75 and 77 and includes the free energy of the free fragments. The effective rate coefficient for the DISC pathway can be estimated by making the pseudosteady state approximation for the caged complex, ignoring the possibility of forming the free fragments. We found that the barrier to form the reactant or product from the caged complex were nearly the same for reaction 77; for simplicity and due to the uncertainties involved, we assume that the barriers to form either isomer from the caged complex are equal. Performing the PSSA analysis with these assumptions leads to the effective rate coefficient expression: $k_{eff}^{DISC} = {}^1/_2 k_{react \rightarrow caged}$, essentially saying that half of the caged complex forms the product, and the rest falls back to the reactant. The resulting rate coefficients for reactions 75 and 77 were calculated to be 6.7 s^{-1} and 3.7×10^{-4} s^{-1}, respectively.

The direct TS rate coefficient at the MP2/CBSB7 level for the isomerization of NH_2ONO to $ONNH_2O$ was found to be 3.9×10^1 s^{-1}, which is faster than the DISC rate coefficient in this case. It is also noticeably faster than the direct rate coefficient calculated via B3LYP/CBSB7 (reaction 84 in Table 3) because the MP2 barrier is $\sim$4.5 kcal/mol smaller. The computational methodology may have a large impact on the estimated rate coefficients, highlighting the significant uncertainty in the methodology. All methods give a small rate coefficient for reaction 77, indicating that $ONNH_2OH^+$ and NH_2OHNO^+ react by other routes, primarily deprotonation reactions. This shows that these DISC reactions will likely not be an important part of the model and justifies not refining the rate estimates further. In general, DISC reactions will become important when the barrier to form the caged complex is significantly lower than the barrier for the concerted isomerization.

Modeling Results and Discussion. The system of interest has been studied by several researchers, mainly concerned with product yields and ignition time, which are generally used to define the stability of the system. The ignition event is characterized by a precipitous decrease in the hydroxylamine concentration and a concurrent increase in the nitrous acid and/ or nitrous oxide concentrations. Pembridge and Stedman[12] and Bennett et al.[36] have collected yield and ignition time data for the system at 298 K and over a limited range of initial nitric acid, nitrous acid, and hydroxylamine concentrations. These data
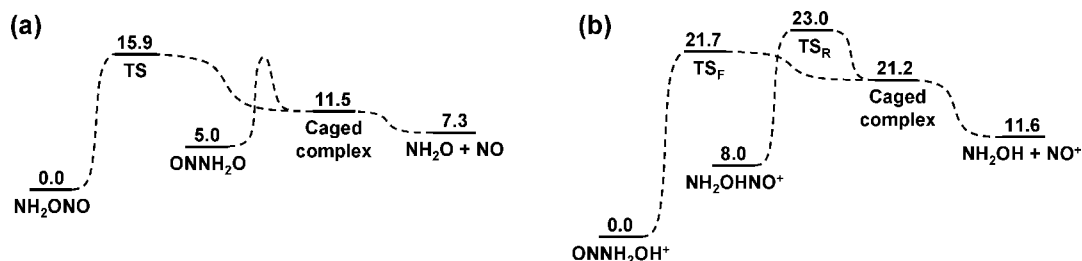
Figure 4. Free energy surface for reactions 75 (a) and 77 (b) and dissociation to free products at 298 K and a standard state concentration of 0.0409 M. Units: kcal/mol.

TABLE 5: Corrections to Thermochemistry To Force Agreement with pK_A Values

| species | $\Delta H_{f,solution}$(298K) (kcal/mol) | | | |
	correction	modified value	expt	source
H$_2$O	0.2	−68.3	−68.3	ref 38
HONO	0.7	−28.5	−28.5	ref 38
NO$_2^-$	0.7	−117.3	−118.0	refs 38 and 11
HONO$_2$	−3.0	−47.3	−49.6	ref 38
NO$_3^-$	1.0	−142.2	−142.0	refs 38 and 11
NH$_2$OH	2.0	−23.5	−23.5	ref 38
NH$_3$OH$^+$	0.0	60.7	60.2	refs 38 and 11
N$_2$H$_4$	3.5	8.2	8.2	ref 38
N$_2$H$_5^+$	−1.0	88.7	91.2	refs 38 and 11

will be used as a metric for the kinetic model prediction, and to identify which model parameters would need to be changed to achieve agreement.

The model has four major parts: the reaction mechanism, basic thermochemistry, rate coefficients, and activity coefficients. Two modeling results will be presented, including a model where the ab initio thermochemistry has been modified to match experimental acid/base equilibria and another with modified rate and thermodynamics parameters to best match the experimental results. Model sensitivity analysis will show that there are only a small number of rate coefficients and thermochemical parameters that significantly affect the nitrous acid yield and the ignition time.

Thermochemistry and Rate Coefficient Corrections. The pK_A values of the major acids in the system are known accurately, so it is prudent to force the estimated thermochemistry to match with the well established experimental values when modeling the system. This was accomplished by altering the ΔH_f of either the conjugate acid or base. If experimental data were available for the ΔH_f of species involved in the reaction, then the correction was made to improve the agreement of both the estimated ΔH_f and pK_A with experimental data. The ionic species were modified with more prejudice because both the ab initio solvation model and the experimental data are likely to have larger errors for charged species than for neutral species. The corrections to the thermochemistry can be found in Table 5. In addition to these changes, the enthalpy of formation of NO$^+$ was decreased by 5 kcal/mol, to match the experimental free energy change for the HONO + H$_3$O$^+$ ⇌ NO$^+$ + 2H$_2$O equilibrium of 8.9 kcal/mol.[37] Any further corrections to the thermochemistry needed to match the experimentally observed HONO yields and ignition times will be discussed later.

Another important correction is for the activity coefficients of the major species, in this case HONO$_2$, H$_2$O, H$_3$O$^+$, and NO$_3^-$. Fortunately, nitric acid systems have been characterized by a number of researchers and several estimates for the activity coefficients in a nitric acid/water system are available.[18,39–43] Ideally, one would like to have the individual activity coefficients for each species; however, typically a mean ionic activity

coefficient is measured for ionic species. This represents the geometric mean of the activity coefficients of the counterions but tells nothing of the individual behavior of the ions. The activity coefficients of undissociated nitric acid and water can be found in the literature.[18] There are several sources for the mean ionic activity coefficient for which the data do not agree, so there may be considerable uncertainty. This will lead to further uncertainty in the predictions of the kinetic model, but the nonideality must be accounted for to achieve meaningful results. The activity coefficients used in the models were fitted to data from Davis and de Bruin[18] for undissociated nitric acid and water, and to the mean ionic activity coefficient reported by Hamer and Wu[40] for both NO$_3^-$ and H$_3$O$^+$. Details on exactly how these activity coefficients were built into the model can be found in the Supporting Information. Activity coefficients are the last major piece required to achieve a realistic model. The infinite-dilution activity coefficients are often overlooked but are especially important when the aqueous system has a significant concentration of solutes. Ignoring these terms effectively means neglecting the solute−solvent interaction change when the solvent changes from pure water (as in the solvation model) to the actual solvent mixture (as in the real aqueous nitric acid system).

The limited experimental rate data available for comparison suggest that the calculated rate coefficients are even more uncertain than the calculated thermochemistry. It is well understood that gas-phase computational estimates of transition state energies generally have larger errors than the associated equilibrium structures, and there is no reason to believe this would change for solution-phase estimates. It is likely that the errors in reaction barriers would be even larger in solution because the parameters in the solvation models have been tuned to match equilibrium structures and several specific solvent effects known to affect rate coefficients are neglected in continuum models.

Initial Model. The full system of differential equations was solved using the thermochemistry estimates and ab initio rate coefficient predictions. An initial, minimally modified model is presented first, which leads into the sensitivity discussion and the further refinements presented later. The barrier for reaction 81, the electron transfer between NH$_2$O and NO$_2$, was the only additional alteration to the model (besides those mentioned in the previous section) and was taken to be 11 kcal/mol for this model. This assumed value lies well within the believed accuracy of our previously described estimate. The value of this parameter significantly affects the HONO yield, as will be shown in the sensitivity analysis. The initial model shows the ability to reproduce some of the experimental yield data, keeping in mind that the barrier of reaction 81 was adjusted to fit the experimental HONO yield for the following initial condition: [NH$_2$OH]$_0$ = 0.012 M, [HONO]$_0$ = 4 × 10^{-5} M, [HONO$_2$]$_0$ = 3 M, [O$_2$]$_0$ = 1 × 10^{-4} M, and T = 298 K. For all models, the

Oxidation of Hydroxylamine by Aqueous Nitric Acid

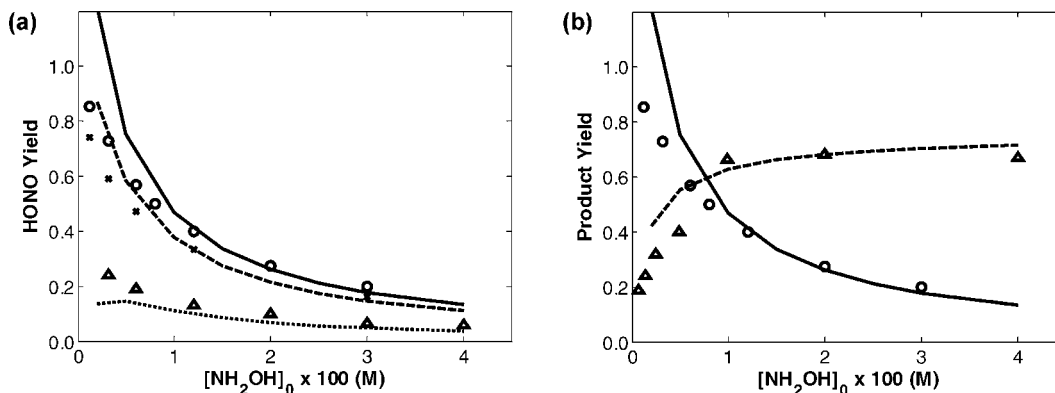*J. Phys. Chem. A, Vol. 112, No. 33, 2008* **7589**

Figure 5. Initial model: (a) Nitrous acid yield as a function of initial hydroxylamine concentration for an initial nitrous acid concentration of 4×10^{-5} M (○ and solid line), 0.001 M (× and dashed line), and 0.004 M (△ and dotted line). (b) Nitrous acid yield (○ and solid line) and corrected nitrous oxide yield (△ and dashed line) as a function of initial hydroxylamine concentration for an initial nitrous acid concentration of 4×10^{-5} M. Markers indicate experimental data, and lines give the model results. The corrected N_2O yield is the sum of the Henry's Law corrected experimental N_2O and N_2 yields; see text for details. Experimental data from ref 36. $[NO_3^-]_0 = 1$ M for these results.

initial concentration of all other species was taken to be zero. This may not be an accurate assumption given the nitric acid solution will likely have a variety H/N/O species present in small but appreciable quantities; this is address briefly in the sensitivity analysis.

The product yield results are shown in Figure 5 for varying initial hydroxylamine and nitrous acid concentrations. The results are very reasonable for this metric. In Figure 5b, the corrected nitrous oxide yield was defined as the sum of the Henry's Law corrected experimental N_2 and N_2O yields.[36] The nitrogen and nitrous oxide yields are combined because the model does not contain a molecular nitrogen formation pathway, and it is believed that the nitrogen is produced through an offshoot of the scavenging pathway at low hydroxylamine concentrations.[36] Therefore, we assumed that any nitrogen produced will reduce the nitrous oxide yield, and not affect the nitrous acid yield. The experimental N_2O and N_2 yields of Bennett et al. were measured through a combination of the pressure above the solution and gas chromatography. The mass balance suggests Bennett et al. did not take vapor−liquid equilibrium into account (a significant amount of N_2O is dissolved in the liquid phase). This was corrected using eq 19, showing the relationship between the effective solution-phase concentration (as would be given by our single-phase model), the gas-phase concentration, and the Henry's Law constant (**H**) with units of $(mol/L)_{soln}/(mol/L)_{gas}$. The Henry's Law constants are 0.61 for N_2O and 0.015 for N_2.[44] The liquid/gas volume ratio was not specified in the original paper and was assumed to be 1:1 for this analysis. The adjusted values agree much better with the modeling results, and they also provide a more complete material balance.

$$C_{liq}^{eff} = \frac{N_{total}}{V_{liq}} = \frac{V_{liq}C_{gas}\mathbf{H} + V_{gas}C_{gas}}{V_{liq}} = C_{gas}\left(\mathbf{H} + \frac{V_{gas}}{V_{liq}}\right)$$

(19)

Despite reasonable agreement with yield data as a function of the initial hydroxylamine concentration, the initial model fails to reproduce other metrics, particularly the ignition time and HONO yield as a function of acidity. The temporal absorption profile corresponding to HONO is given in Figure 6 for the experimental data[12] and model results. The model concentration was converted to absorbance using an extinction coefficient of 50 M^{-1} cm^{-1} and a path length of 1 cm.[36] The model predicts an ignition time that is approximately 2 orders of magnitude
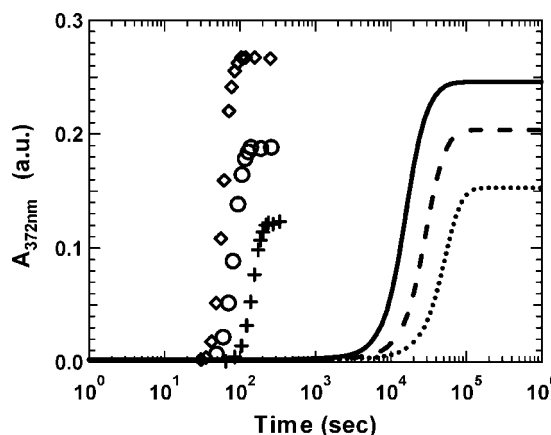

Figure 6. Initial model: absorbance profiles for nitrous acid (372 nm) for different initial hydroxylamine concentrations: 0.012 M (◇ and solid line); 0.006 M (○ and dashed line); 0.003 M (+ and dotted line). Markers indicate experimental data, and lines give the model results. Experimental data and $\epsilon = 50$ M^{-1} cm^{-1} from ref 36. $[NO_3^-]_0 = 1$ M for these results.

larger than experiment, which is a significant deficiency for a model that we would like to use to predict the stability of the system. However, the trends match very well, and if the ignition time could be shifted to shorter times without affecting the yield, the model results would be reasonable. Fortunately, there are a number of ways in which the ignition time can be shortened without significantly affecting the yield. Increasing the rate coefficient of reaction 22 ($NH_3OH^+ \cdot H_2O + NO^+ \rightarrow NH_3ONO^+ + H_3O^+$) has the largest potential effect. The thermochemistry of species which participate in these reactions also can significantly affect the timing. The species thermochemistry with the most sensitivity are NO^+, NH_3ONO^+, and NO_2, ignoring species present in the major acid/base equilibria. Many combinations of rate coefficient and thermochemistry changes can yield the desired ignition time, so the choice of which parameters to modify is somewhat arbitrary. Despite having these handles at our disposal, it was not possible with modest perturbations to achieve a better agreement with experimental data than approximately 1 order of magnitude in ignition time. Although it would be possible to force agreement with more and/or larger changes, we view such changes as too arbitrary to present here (though given the large uncertainties in some of the model parameters, quite large adjustments may be correct).

The other major discrepancy is the acidity dependence of the nitrous acid yield, which experimentally shows nonmonotonic
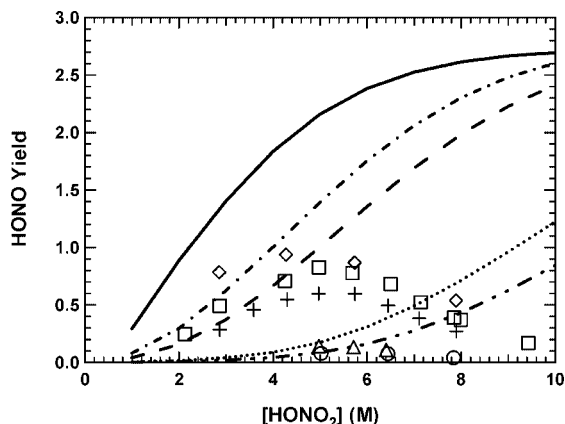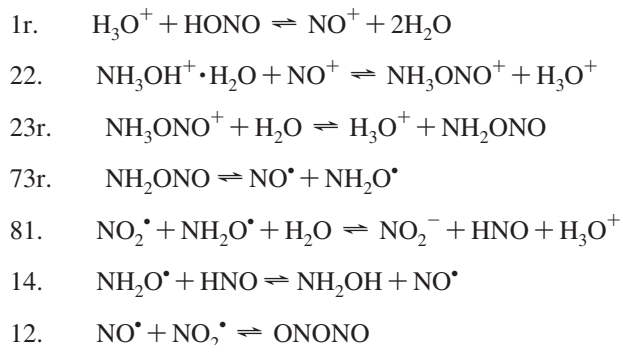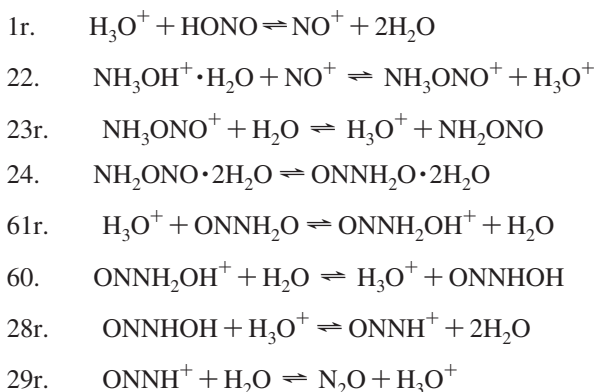
Figure 7. Initial model: nitrous acid yield as a function of initial acid concentration at various initial hydroxylamine concentrations: 0.001 M ($\Diamond$ and solid line); 0.005 M ($\square$ and dash-dot line); 0.01 M (+ and dashed line); 0.1 M ($\triangle$ and dotted line); 0.2 M ($\bigcirc$ and dash-dot-dot line). Markers indicate experimental data, and lines give the model results. Experimental data from ref 12.

behavior as the concentration of nitric acid is increased.[12] The model does a poor job of capturing this trend, as shown in Figure 7. As with the ignition time, this disagreement could not be rectified by modest changes in the parameter values. Sensitivity analyses performed at nitric acid concentration of 3 and 8 M showed that no single perturbation in species thermochemistry could cause the yield to decrease at 8 M and stay the same or increase at 3 M. The model predictions do show a nonmonotonic behavior, but the peak in the yield curves occurs at nitric acid concentrations larger than 10 M, and systems having a larger initial hydroxylamine concentrations peaked at higher nitric acid concentrations. This trend is similar to the experimental data, but offset by a large amount in yield and nitric acid concentration. This problem may be indicative of deficiencies in activity coefficient predictions for the major species and/or ignoring the infinite dilution activity coefficients of the minor species in nitric acid.

Despite the deficiencies in the initial model, we can examine the reaction fluxes to determine the autocatalytic and scavenging pathways demonstrated by this model. The autocatalytic pathway is shown below, where the NO_2 is supplied by a combination of reactions 6, 7, and 19. The branching between the two pathways mainly occurs with the reactions of NH_2ONO, where dissociation of this species leads to the autocatalytic products and isomerization leads to the scavenging products. As with any complicated mechanism, there are other minor interactions between the two branches, but the majority of the behavior can be characterize by this species. Although the branching occurs with NH_2ONO in this case, the rate limiting reaction in the autocatalytic branch appears to be reaction 81.

1r. $H_3O^+ + HONO \rightleftharpoons NO^+ + 2H_2O$

22. $NH_3OH^+ \cdot H_2O + NO^+ \rightleftharpoons NH_3ONO^+ + H_3O^+$

23r. $NH_3ONO^+ + H_2O \rightleftharpoons H_3O^+ + NH_2ONO$

73r. $NH_2ONO \rightleftharpoons NO^\bullet + NH_2O^\bullet$

81. $NO_2^\bullet + NH_2O^\bullet + H_2O \rightleftharpoons NO_2^- + HNO + H_3O^+$

14. $NH_2O^\bullet + HNO \rightleftharpoons NH_2OH + NO^\bullet$

12. $NO^\bullet + NO_2^\bullet \rightleftharpoons ONONO$

13. $ONONO + H_2O \rightleftharpoons HONO + HONO$

The dominant nitrous acid scavenging pathway predicted by the initial model is presented below. There are other minor channels that contribute to the scavenging, but all other fluxes are several orders of magnitude less. Under these conditions, reaction 24 is the yield-limiting step in the scavenging reaction, whereas reactions 1 and 22 govern the time-evolution of the system under these conditions.

1r. $H_3O^+ + HONO \rightleftharpoons NO^+ + 2H_2O$

22. $NH_3OH^+ \cdot H_2O + NO^+ \rightleftharpoons NH_3ONO^+ + H_3O^+$

23r. $NH_3ONO^+ + H_2O \rightleftharpoons H_3O^+ + NH_2ONO$

24. $NH_2ONO \cdot 2H_2O \rightleftharpoons ONNH_2O \cdot 2H_2O$

61r. $H_3O^+ + ONNH_2O \rightleftharpoons ONNH_2OH^+ + H_2O$

60. $ONNH_2OH^+ + H_2O \rightleftharpoons H_3O^+ + ONNHOH$

28r. $ONNHOH + H_3O^+ \rightleftharpoons ONNH^+ + 2H_2O$

29r. $ONNH^+ + H_2O \rightleftharpoons N_2O + H_3O^+$

Understanding this rather complex kinetic system requires careful analysis, as is discussed in the following sections.

Sensitivity Analysis. The first-order sensitivities were estimated by finite differences, changing the rate coefficients, the enthalpies of formation, and the initial conditions. These parameters were perturbed and the change in the nitrous acid yield, hydroxylamine conversion, and "ignition time" were monitored to determine the species/reactions most important to the reacting system. Yields were defined as the change in concentration from the initial condition divided by the initial hydroxylamine concentration. The "ignition" time was defined as the time until the half-maximum in the HONO concentration profile and is undefined if the concentration never increases above the initial value, e.g., negative HONO yields. The initial condition was chosen to be $[NH_2OH]_0 = 0.012$ M, $[HONO]_0 = 4 \times 10^{-5}$ M, $[HONO_2]_0 = 3$ M, $[O_2]_0 = 1 \times 10^{-4}$ M, and $T = 298$ K, a condition where many experimental data are available. The acid/base equilibria for $HONO_2$ is fast, and $[HONO_2]_0 = 3$ M is approximately equivalent to $[H_3O^+]_0 = 3$ M and $[NO_3^-]_0 = 3$ M. The rate coefficients were increased/decreased by a factor of 5 and the enthalpies of formation were increased/decreased by a 0.1 kcal/mol in these analyses. The full sensitivity and flux analyses of all models can be found in the Supporting Information. A model is often most sensitive to species or reactions that are omitted in the model; despite efforts to include many reasonable species and reactions, no complex mechanism can ever be deemed complete.

The system is only sensitive to a handful of reactions and thermochemical parameters. Relatively small perturbations in the system parameters will likely not change the main reaction channel but may change which reaction in the pathway is rate-limiting and most influential to the nitrous acid yield. When thinking about the sensitivity, it is also important to remember the autocatalytic nature of the reaction and how it may affect the sensitivity results. In this type of reaction, there are two extremes, purely autocatalytic and purely stable, and the intermediate regime where the autocatalytic and scavenging processes are somewhat balanced. If the model predicts a purely autocatalytic response, then the HONO yield will always be high and constant, no matter what system parameters are varied, and all of the sensitivity values will be near-zero. A similar
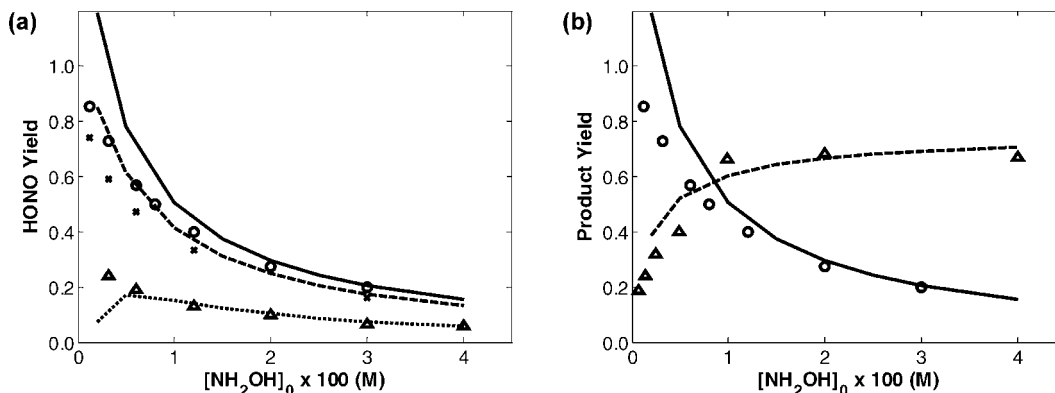
Oxidation of Hydroxylamine by Aqueous Nitric Acid

J. Phys. Chem. A, Vol. 112, No. 33, 2008 **7591**

Figure 8. Final model: (a) Nitrous acid yield as a function of initial hydroxylamine concentration for an initial nitrous acid concentration of: 4×10^{-5} M ($\bigcirc$ and solid line); 0.001 M ($\times$ and dashed line); 0.004 M ($\triangle$ and dotted line). (b) Nitrous acid yield ($\bigcirc$ and solid line) and corrected nitrous oxide yield ($\triangle$ and dashed line) as a function of initial hydroxylamine concentration for an initial nitrous acid concentration of 4×10^{-5} M. Markers indicate experimental data, and lines give the model results. The corrected N_2O yield is the sum of the Henry's Law corrected experimental N_2O and N_2 yields; see text for details. Experimental data from ref 36. $[NO_3^-]_0 = 1$ M for these results.

behavior would be seen for a purely scavenging (stable) system with a small HONO yield. However, in the parameter space in between, minor changes in the system parameters can elicit large changes in the yield, which is where the true physical system is known to exist.

The sensitivity of the initial model to the various parameters was examined. The main objective of this analysis was to find the parameters that are most important to the autocatalytic and scavenging pathways. The change in HONO yield was used as the main metric in determining the system sensitivity to a given parameter. The two most influential rate coefficients were those of reactions 81 and 24, indicating that they are the rate limiting reactions and govern the branching ratio. Perturbing reactions 74 and 61 also showed a moderate ability to change the HONO yield, though the system sensitivity to these reactions is about an order of magnitude less than reactions 81 and 24. In the thermochemistry sensitivity analysis, many of the important species are involved in the acid/base equilibria that were fixed. This is not unexpected because these equilibria govern the concentrations of major species within the system; however, these thermochemical parameters cannot be changed independently because it would violate the experimental pK_A values mentioned earlier. For the initial model, the HONO yield is most sensitive to the thermochemistry of H_2O, H_3O^+, HONO, $ONNH_2O$, NO_3^-, NH_2ONO, NH_2O, and NO_2. Many of these species are also present in the reactions that had the highest sensitivity.

The sensitivity of the initial model to changes in the initial concentration of minor species was also investigated. The initial concentrations of $HONO_2$, NH_2OH, HONO, and O_2 were fixed, and the initial concentrations of other species in the systems were individually changed from zero to 1×10^{-5}, 1×10^{-4}, or 1×10^{-3} M. Although the initial concentration of O_2 was fixed in this analysis, a cursory analysis showed that it had little effect on the model within its reasonable range; the chosen value of 1×10^{-4} M represents a reasonable upper bound based on equilibrium arguments.[45] The detailed effect on the system behavior is given in the Supporting Information and is summarized here. It is worth noting that the perturbed concentrations will likely be absurdly large for many of the intermediates, but this analysis is meant to indicate the worst case scenarios. None of the single perturbations significantly affected the HONO yield of the system at any of the initial concentration levels. For the initial concentration level of 1×10^{-5} M, the "ignition" time was changed by no more than 7%, with the time from 5% to

95% of the HONO yield remaining essentially fixed. When the initial concentration level was set to 1×10^{-4} M, the ignition time decreased by up to 30%, and the time from 5% to 95% of the HONO yield changing by less than 2%. The concentration value of 0.001 M could elicit even larger changes but is unrealistic for nearly all of the minor species. The interplay of combinations of minor species having a significant concentration could potentially be more important, but the full combinatorial exercise was not undertaken for obvious reasons. A simple Monte Carlo analysis was performed by allowing each minor species' initial concentration to randomly vary between 1×10^{-15} and 1×10^{-6} M. The initial concentration vector was unique for each of the 3000 MC steps; however, given the 40-dimensional space, these steps represent a miniscule part of the variable space. The change in yield and ignition time was calculated relative to the normal case of assuming a zero initial concentration for minor species. The absolute values of the HONO yield change and ignition time change for all cases were less than 0.0001 and 300 s, respectively, out of base values of 0.32 and 14600 s.

Final Model. Although the initial model fails to reproduce some of the data, we had fixed the thermochemistry of the major acid/base species. As one may expect, the thermochemistry of these species is important not only to the acid/base equilibria but also to other reactions and system behavior in general. If the experimental absolute enthalpy of formation data have large uncertainties, then we may be forcing incorrect species thermochemistry even though the pK_A values are correct. In the final model, the thermochemistry of nitric acid and the nitrate ion were modified, though still enforcing the experimental pK_A. Instead of the corrections of -3 and $+1$ kcal/mol for $HONO_2$ and NO_3^- shown in Table 5, we introduced corrections of $+2$ and $+6$ kcal/mol; the other thermochemistry corrections were the same as before. Because the $HONO_2/NO_3^-$ changes tend to make the system more autocatalytic, the E_A value for reaction 24 was decreased by 3 kcal/mol and the E_A value for reaction 81 was set to 15.5 kcal/mol to achieve the proper yield.

The modeling results for the nitrous acid and nitrous oxide yields are shown in Figure 8. These model predictions are essentially identical to those presented earlier, matching the experimental yield measurements well. The acidity dependence of the nitrous acid yield for this model is shown in Figure 9. Here the model-predicted HONO yield follows the same nonmonotonic trend as the experimental data, showing a distinctive peak as the initial concentration of nitric acid is
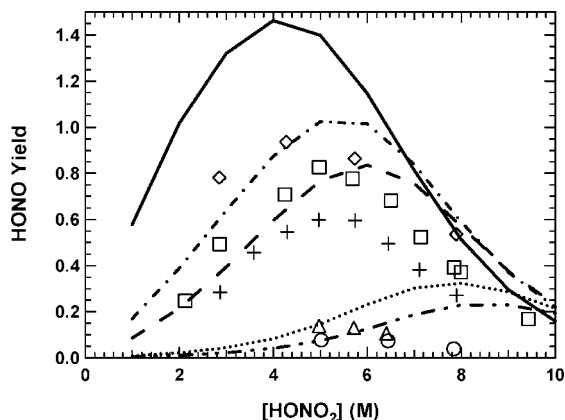
Figure 9. Final model: nitrous acid yield as a function of initial acid concentration at various initial hydroxylamine concentrations: 0.001 M ($\diamond$ and solid line); 0.005 M ($\square$ and dash-dot line); 0.01 M (+ and dashed line); 0.1 M ($\triangle$ and dotted line); 0.2 M ($\bigcirc$ and dash-dot-dot line). Markers indicate experimental data, and lines give the model results. Experimental data from ref 12.
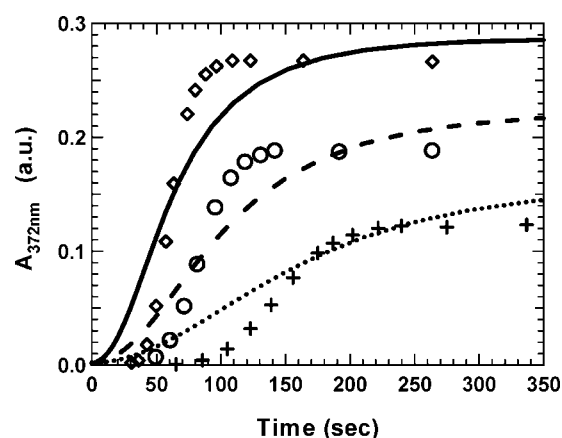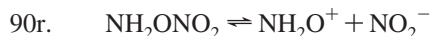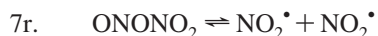

Figure 10. Final model with the E_A for reaction 9 decreased by 5 kcal/mol. Absorbance profiles for nitrous acid (372 nm) for different initial hydroxylamine concentrations: 0.012 M ($\diamond$- and solid line); 0.006 M ($\bigcirc$ and dashed line); 0.003 M (+ and dotted line). Markers indicate experimental data, and lines give the model results. Experimental data and $\epsilon = 50$ M^{-1}cm^{-1} from ref 36. $[NO_3^-]_0 = 1$ M for these results.
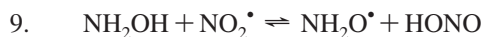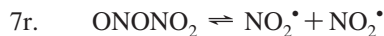
increased. This is a direct result of the modification of the nitric acid thermochemistry, which depressed and shifted the position of the peak in HONO yield. The autocatalytic mechanism in this case is essentially the same as was seen in the initial model.

The ignition time predicted by the final model is still about 2 orders of magnitude too slow with only the corrections mentioned above. This can be partially corrected by decreasing the NO$^+$ enthalpy of formation further and/or by increasing the rate of reaction 22 without a significant impact on the product yields or the mechanism. Another change that could be employed is decreasing the E$_A$ for reaction 9, NH$_2$OH + NO$_2$ → NH$_2$O + HONO, by 5.0 kcal/mol. This yields a rate coefficient of 3×10^7 M^{-1} s^{-1} and changes the ignition time from about 17000 to 60 s, which is similar to the experimental data. The barrier for reaction 9 was predicted to be ∼6 kcal/mol, so 5 kcal/mol is a significant change. Alternatively, fast electron transfer for the NH$_2$OH + NO$_2$ → NH$_2$OH$^+$ + NO$_2^-$ reaction would have essentially the same effect on the kinetics, but this would require a barrier much lower than that predicted by simple Marcus Theory. A comparison of the adjusted model and experimental HONO traces are given in Figure 10. The change to reaction 9 does not materially affect the model yields presented in Figure 8 and Figure 9.

Although only modestly affecting the product distributions, accelerating reaction 9 results in major changes in the scavenging and autocatalytic pathways. The mechanism no longer relies on the formation of NO$^+$ and reaction 22 to drive the evolution, but instead almost the entire flux is channeled through reaction 9. The new dominant autocatalytic mechanism is given below. Minor channels that contribute species to the main pathway have been omitted. The initial part of the autocatalytic mechanism is similar to what was previously proposed by Pembridge and Stedman; however, our model does not indicate that reaction 13 is a significant source of nitrous acid formation, as proposed by Pembridge and Stedman. In fact, the model flux analysis shows that there is a large reverse flux for reaction 13, which generates ONONO and ultimately serves as a source of NO radicals for the scavenging pathway.

19r.   HONO$_2$ + HONO $\rightleftharpoons$ H$_2$O + ONONO$_2$

7r.   ONONO$_2$ $\rightleftharpoons$ NO$_2^\bullet$ + NO$_2^\bullet$

9.   NH$_2$OH + NO$_2^\bullet$ $\rightleftharpoons$ NH$_2$O$^\bullet$ + HONO

81.   NO$_2^\bullet$ + NH$_2$O$^\bullet$ + H$_2$O $\rightleftharpoons$ NO$_2^-$ + HNO + H$_3$O$^+$

41.   NO$_2^\bullet$ + NH$_2$O$^\bullet$ $\rightleftharpoons$ NH$_2$ONO$_2$

90r.   NH$_2$ONO$_2$ $\rightleftharpoons$ NH$_2$O$^+$ + NO$_2^-$

14.   NH$_2$O$^\bullet$ + HNO $\rightleftharpoons$ NH$_2$OH + NO$^\bullet$

The new scavenging pathway is given below, which is the same as before once ONNH$_2$O is formed. As mentioned above, the source of NO radicals in the scavenging pathway is mainly from the decomposition of ONONO following the reverse of reaction 13.

19r.   HONO$_2$ + HONO $\rightleftharpoons$ H$_2$O + ONONO$_2$

7r.   ONONO$_2$ $\rightleftharpoons$ NO$_2^\bullet$ + NO$_2^\bullet$

9.   NH$_2$OH + NO$_2^\bullet$ $\rightleftharpoons$ NH$_2$O$^\bullet$ + HONO

73.   NO$^\bullet$ + NH$_2$O$^\bullet$ $\rightleftharpoons$ NH$_2$ONO

24.   NH$_2$ONO·2H$_2$O $\rightleftharpoons$ ONNH$_2$O·2H$_2$O

This exercise of parameter adjustment was not meant as an attempt to find the correct mechanism; because of the uncertainties in the rate and thermochemical parameters, there is not enough information to uniquely determine which pathways dominate. The purpose is to show that fairly good agreement with experimental data can be obtained with a few small changes in the parameters, well within the uncertainty of the estimates. There are many ways that the parameters could be altered to achieve partial agreement with the data, even yielding different autocatalytic pathways; two of these likely autocatalytic pathways are presented here. Given the uncertainties in the ab initio thermochemistry and rate coefficients, we cannot differentiate between these two mechanisms or prove that either is dominant in the physical system. It is hoped that these hypotheses and rate coefficient calculations will help to guide experimental work attempting to draw a more precise picture of the true scavenging and autocatalytic pathways.

Conclusion

A general procedure for estimating solution-phase rate coefficients from ab initio calculations is presented. Traditional transition state theory procedures are outlined as they apply to solution-phase estimates, taking care to address standard states

and activity coefficients correctly, as discussed in the Supporting Information. A method was proposed to estimate rate coefficients for dissociative isomerizations in a solvent cage, drawing ideas from variational transition state theory. The importance of including explicit solvent molecules in particular classes of reactions was shown. Unfortunately, a lack of meaningful experimental rate coefficient data precludes us from drawing conclusions about the absolute accuracy of the TST or caged-reaction rate coefficient estimates. However, given the error present in the thermochemistry, it is unlikely the activation barriers are more accurate than 2 kcal/mol, which translates to at least 1 order of magnitude uncertainty in the rate coefficients at 298 K.

The hydroxylamine/nitric acid/nitrous acid system was modeled using a proposed 90-reaction mechanism, taking into account several types of chemistry. The initial, minimally modified model showed some ability to reproduce experimental yield data; however, the time scale of the reaction and the acidity dependences of the yields could not be rectified with a few small perturbations in the parameters. The acidity dependence could be accurately modeled by making changes to the thermochemistry of nitric acid and the nitrate ion, while constraining them to be consistent with the known pK_A. Potential autocatalytic and scavenging pathways were proposed, although a definitive mechanism cannot be determined due to the uncertainties in the predicted rate coefficients and thermochemistry.

More importantly, we have highlighted the areas in which major improvements need to be made to successfully model a complex solution-phase system. The most important advances will come from more accurate, yet computationally efficient, solvation models that allow accurate equilibrium constants and reaction barriers to be estimated. New theories more precisely describing atypical reaction types that are found in condensed-phase systems will also be needed to fully understand condensed-phase dynamics. A reliable methodology for estimating activity coefficients of stable species and transition states, including at infinite-dilution in multicomponent mixtures, will also be critical when studying concentrated aqueous solutions. Many researchers are currently working on these tasks, and we applaud their efforts; however, the community must make significantly more progress before ab initio prediction of complex aqueous system behavior is a reality.

Supporting Information Available: Geometries for each of the transition state structures used to calculate rate coefficients, additional details regarding the partition functions values and estimates of the DISC rate coefficients, discrete sensitivity analyses and flux analyses for each model discussed in the text, further discussion of diffusion-limited rate estimates, details of the electron-transfer-rate estimates, major species activity coefficient data and fitting, and data from the B3LYP/MP2 reaction barrier comparison. A detailed account of the assumptions needed to derive solution-phase equilibrium expressions and transition state theory is also included. This material is available free of charge via the Internet at http://pubs.acs.org.

References and Notes

(1) Smith, G. P.; Golden, D. M.; Frenklach, M.; Moriarty, N. W.; Eiteneer, B.; Goldenberg, M.; Bowman, C. T.; Hanson, R. K.; Song, S.; William C. Gardiner, J.; Lissianski, V. V.; Qin, Z. GRI-Mech 3.0; http://www.me.berkeley.edu/gri_mech/, 2004.

(2) Curran, H. J.; Gaffuri, P.; Pitz, W. J.; Westbrook, C. K. *Combust. Flame* **2002**, *129*, 253.

(3) Harding, L. B.; Klippenstein, S. J.; Miller, J. A. *J. Phys. Chem. A* **2008**, *112*, 522.

(4) Moskaleva, L. V.; Lin, M. C. *Proc. Combust. Inst.* **2000**, *28*, 2393.

(5) Harrington, J. E.; Smith, G. P.; Berg, P. A.; Noble, A. R.; Jeffries, J. B.; Crosley, D. R. *Proc. Combust. Inst.* **1996**, *26*, 2133.

(6) Bozzelli, J. W.; Dean, A. M. *Int. J. Chem. Kinet.* **1995**, *27*, 1097.

(7) Matheu, D. M.; Dean, A. M.; Grenda, J. M.; Green, W. H., Jr *J. Phys. Chem. A* **2003**, *107*, 8552.

(8) Klamt, A.; Schuurmann, G. *J. Chem. Soc., Perkin Trans. 2* **1993**, 799.

(9) Andzelm, J.; Kolmel, C.; Klamt, A. *J. Chem. Phys.* **1995**, *103*, 9312.

(10) Klamt, A.; Eckert, F.; Diedenhofen, M.; Beck, M. E. *J. Phys. Chem. A* **2003**, *107*, 9380.

(11) Ashcraft, R. W.; Raman, S.; Green, W. H. *J. Phys. Chem. B* **2007**, *111*, 11968.

(12) Pembridge, J. R.; Stedman, G. *J. Chem. Soc., Dalton Trans.* **1979**, 1657.

(13) Bourke, G. C. M.; Stedman, G. *J. Chem. Res., Synop.* **1999**, 684.

(14) Bourke, G. C. M.; Stedman, G. *J. Chem. Soc., Perkin Trans. 2* **1992**, 161.

(15) Steinfeld, J. I.; Francisco, J. S.; Hase, W. L. *Chemical Kinetics and Dynamics*, 2nd ed.; Prentice Hall: Upper Saddle River, NJ, 1998.

(16) Marx, D.; Tuckerman, M. E.; Hutter, J.; Parrinello, M. *Nature* **1999**, *397*, 601.

(17) Cavagnat, D.; Lassegues, J. C. *Solid State Ionics* **1991**, *46*, 11.

(18) Davis, W., Jr.; de Bruin, H. J. *J. Inorg. Nucl. Chem.* **1964**, *26*, 1069.

(19) Klamt, A. *COSMO-RS: From Quantum Chemistry to Fluid Phase Thermodynamics and Drug Design*; Elsevier: Amsterdam, 2005.

(20) Klamt, A.; Jonas, V.; Burger, T.; Lehrenz, J. C. W. *J. Phys. Chem. A* **1998**, *102*, 5074.

(21) Eckert, F.; Klamt, A. *AIChE J.* **2002**, *48*, 369.

(22) Kelly, C. P.; Cramer, C. J.; Truhlar, D. G. *J. Chem. Theory Comput.* **2005**, *1*, 1133.

(23) Chamberlin, A. C.; Cramer, C. J.; Truhlar, D. G. *J. Phys. Chem. B* **2006**, *110*, 5665.

(24) Cannon, R. D. *Electron Transfer Reactions*; The Butterworth Group: London, 1980.

(25) Marcus, R. A. *Discuss. Faraday Soc.* **1960**, *29*, 21.

(26) Marcus, R. A. *J. Chem. Phys.* **1965**, *43*, 679.

(27) Zhou, H.-X.; Szabo, A. *J. Chem. Phys.* **1995**, *103*, 3481.

(28) Forst, W. *J. Phys. Chem.* **1991**, *95*, 3612.

(29) Baer, T.; Hase, W. L. *Unimolecular Reaction Dynamics*; Oxford University Press, Inc.: New York, 1996.

(30) Raman, S.; Ashcraft, R. W.; Vial, M. A.; Klasky, M. L. *J. Phys. Chem. A* **2005**, *109*, 8526.

(31) Bielski, B. H. J.; Cabelli, D. E.; Arudi, R. L.; Ross, A. B. *J. Phys. Chem. Ref. Data* **1985**, *14*, 1040.

(32) Simic, M.; Hayon, E. *J. Am. Chem. Soc.* **1971**, *93*, 5982.

(33) Maurer, P.; Thomas, C. F.; Kissner, R.; Ruegger, H.; Greter, O.; Rothlisberger, U.; Koppenol, W. H. *J. Phys. Chem. A* **2003**, *107*, 1763.

(34) Schwartz, S. E.; White, W. H. Kinetics of Reactive Dissolution of Nitrogen Oxides into Aqueous Solution. In *Trace Atmospheric Constituents*; Schwartz, S. E., Ed.; John Wiley & Sons: New York, 1983; pp 1.

(35) Elliot, A. J.; Simsons, A. S. *Can. J. Chem.* **1984**, *62*, 1831.

(36) Bennett, M. R.; Brown, G. M.; Maya, L.; Posey, F. A. *Inorg. Chem.* **1982**, *21*, 2461.

(37) Ridd, J. H. Diffusion Control and Pre-association in Nitrosation, Nitration, and Halogenation. In *Advances in Physical and Organic Chemistry*; Gold, V., Bethell, D., Eds.; Academic Press: New York, 1978; Vol. 16, pp 1.

(38) Wagner; Evans; Parker; Schumm; Halow; Bailey; Churney; Nuttall, *J. Phys. Chem. Ref. Data* **1982**, 11.

(39) Marcos-Arroyo, M. d. M.; Khoshkbarchi, M. K.; Vera, J. H. *J. Solution Chem.* **1996**, *25*, 983.

(40) Hamer, W. J.; Wu, Y.-C. *J. Phys. Chem. Ref. Data* **1972**, *1*, 1047.

(41) Tamamushi, R. *Bull. Chem. Soc. Jpn.* **1974**, *47*, 1921.

(42) *Properties of Aqueous Solutions of Electrolytes*; Zaytsev, I. D., Aseyev, G. G., Eds.; CRC Press: Boca Raton, FL, 1992.

(43) Dawber, J. G.; Wyatt, P. A. H. *J. Chem. Soc.* **1960**, 3589.

(44) Sander, R. Henry's Law Constants. In *NIST Chemistry Webbook, NIST Standard Reference Database Number 69*; Linstrom, P. J., Mallard, W. G., Eds.; National Institute of Standards and Technology: Gaithersburg, MD, 2005.

(45) Tromans, D. *Ind. Eng. Chem. Res.* **2000**, *39*, 805.

JP711401P